Geometric Singular Perturbation Analysis of Neuronal Dynamics

Jonathan E. Rubin and David Terman
Department of Mathematics
The Ohio State University
Columbus, OH 43210
USA

November 10, 1999

Abstract: In this chapter, we consider recent models for neuronal activity. We review the sorts of oscillatory behavior which may arise from the models and then discuss how geometric singular perturbation methods have been used to analyze these rhythms. We begin by discussing models for single cells which display bursting oscillations. There are, in fact, several different classes of bursting solutions; these have been classified by the geometric properties of how solutions evolve in phase space. We describe several of the bursting classes and then review related rigorous mathematical analysis. We then discuss the dynamics of small networks of neurons. We are primarily interested in whether excitatory or inhibitory synaptic coupling leads to either synchronous or desynchronous rhythms. We demonstrate that all four combinations are possible, depending on the details of the intrinsic and synaptic properties of the cells. Finally, we discuss larger networks of neuronal oscillators involving two distinct cell populations. In particular, we demonstrate how dynamical systems methods can be used to analyze recent models for sleep rhythms and other oscillations generated in the thalamus. The analysis helps to explain the generation of the different thalamic rhythms and the transitions between them, in both of which inhibition plays a crucial role.

Contents

1 Introduction

Oscillations arise throughout the central nervous system [47], [38], [79], [89], [9]. These oscillations have been implicated in the generation of sleep rhythms, epilepsy, parkinsonian tremors, sensory processing, and learning [30], [39], [76], [79], [40]. Oscillatory behavior also arises in such activities as respiration, movement, and secretion [13], [10].

Models for the relevant neuronal networks often exhibit a rich structure of dynamic behavior. The behavior of even a single cell can be quite complicated [11], [13], [82], [83], [31]; an individual cell may, for example, fire repetitive action potentials or bursts of action potentials that are followed by a silent phase of near quiescent behavior [57], [58], [96]. The bursting behavior may wax and wane on a slower time scale [18], [3], [19]. Examples of population rhythms include synchronous behavior, in which every cell in the network fires at the same time, and clustering [27], [28], [44], in which the entire population of cells breaks up into subpopulations or blocks; every cell within a single block fires synchronously and different blocks are desynchronized from each other. Of course, much more complicated population rhythms are also possible [89], [86], [44]. The activity can also propagate through the network in a wave-like manner [41], [19], [88], [29], [61].

In this article, we review numerous recent results in which geometric singular perturbation methods have been used to analyze the dynamics of neuronal networks. Much of the analysis presented is done in the singular limit. Nonetheless, the results are extremely useful for elucidating the roles of network parameters and components in generating various activity patterns.

We begin in Section 2 by considering models for single cells which exhibit bursting oscillations. There are, in fact, several different types of bursting oscillations, and there has been considerable effort in trying to classify the underlying mathematical mechanisms responsible for these oscillations [58], [4], [37]. Models for bursting oscillations contain multiple time scales and this often leads to very interesting issues related to the theory of singular perturbations [46]. Even the simplest bursting models may exhibit exotic behavior, including chaotic dynamics, for certain parameter ranges [11], [83].

In Section 3, we consider models for a pair of mutually coupled cells. The results in this section are complementary to related work in [42]. Each cell will be modeled as a relaxation oscillator; one can view this as a simple depiction of a bursting neuron in which the active phase corresponds to the envelope of a burst's rapid spikes. We only consider a form of coupling between cells that represents chemical synapses, since this is the primary means by which neurons

in the central nervous system communicate with each other. There are, however, many forms of synaptic coupling [40]. It may be excitatory or inhibitory and it may exhibit either fast or slow dynamics. We will be primarily interested in whether excitatory or inhibitory coupling leads to either synchronous or desynchronous rhythms. We will demonstrate that all four combinations are possible, depending on the details of the intrinsic and synaptic properties of the cells.

In Section 4, we consider a larger network of relaxation oscillators with inhibitory and excitatory synaptic coupling, referred to as a *globally inhibitory network* [65], [63]. This network may exhibit both synchronous and clustered solutions and we give sufficient conditions for when each of these rhythms arises. These results help to clarify how the intrinsic properties of individual cells interact with the synaptic properties to produce the emergent population rhythm. Inhibition, for example, may play multiple roles in producing different rhythms. Which rhythms arise depends on how inhibition interacts with intrinsic properties of the neurons; the nature of these interactions depends on the underlying architecture of the network.

Finally, in Section 5, we consider a detailed model for certain sleep rhythms produced in the thalamus. Many of the results in this paper, as well as the particular form of the globally inhibitory network, are motivated by experimental, modeling, and computational studies of these rhythms (see [28] and [22], which provides a review of related works). After describing the rhythms, we discuss in some detail how one models these networks. The model for each cell is based on the Hodgkin-Huxley formalism [33]. We then discuss how the geometric analysis helps to explain the generation of different thalamic rhythms and the transitions between them.

2 Bursting Oscillations

2.1 Introduction

Certain neurons and other excitable cells exhibit bursting oscillations; this behavior is characterized by a silent phase of near steady state resting behavior alternating with an active phase of rapid, spike-like oscillations, as shown in Figure 1. Examples of biological systems which display bursting oscillations include the Aplysia R-15 neuron, insulin secreting pancreatic beta cells, and neurons in the hippocampus, cortex and thalamus. For reviews, see [96], [67], [37].

Figure 1 shows several different types of bursting oscillations. Figure 1A displays an example of *square-wave* bursting. This is characterized by abrupt periodic switching between the quiescent, or silent, phase and the active phase of repetitive firing. Note that the frequency of spikes decreases at the end of the active phase. Figure 1B illustrates *elliptic* bursting. Small amplitude oscillations occur during the silent phase and the amplitude of spikes gradually waxes and wanes.

Finally, Figure 1C displays *parabolic* bursting. The spike rate first increases and then decreases in a parabolic manner.

The mathematical mechanisms responsible for each class of bursting oscillation are described in terms of geometric properties of the corresponding phase space dynamics. The model for each involves multiple time scales and can be written as

$$\begin{aligned} x' &= f(x,y) \\ y' &= \epsilon g(x,y) \end{aligned} \tag{2.1}$$

Here, $x \in R^n$ represents fast variables, while $y \in R^m$ represents slow variables; ϵ is a small singular perturbation parameter. We refer to the first equation in (2.1), with y considered as constant, as the fast subsystem (FS). The silent phase of the bursting solution corresponds to the passage of a trajectory of (2.1) near a manifold of fixed points of (FS). The active phase of repetitive spikes corresponds to the passage of the trajectory near a manifold of periodic solutions of (FS). It is the slow processes which modulate the fast dynamics between these two phases. Different classes of bursting oscillations are distinguished by the mechanisms by which the bursting trajectories switch between the silent and active phases. This is closely related to the global bifurcation structure of the fast subsystem with the slow variables treated as parameters.

We note that models for bursting oscillations may exhibit other types of periodic solutions, as well as more exotic behavior including chaotic dynamics [11], [82], [83]. The models contain multiple time scales and this often leads to very interesting issues related to the theory of singular perturbations. For example, homoclinic orbits usually play an important role in the generation of these rhythms; the active phase of rapid oscillations may either begin or end (or both) as the bursting trajectory crosses a homoclinic point. At these points, standard singular perturbation methods may break down, so more delicate analysis is required. Moreover, the homoclinic orbits are often directly responsible for the generation of chaotic dynamics [82], [83].

In the next section, we describe the mathematical mechanisms responsible for the three classes of bursting oscillations shown in Figure 1. The description is quite heuristic; however, the formal constructions are extremely useful in understanding what geometric ingredients are needed to generate a particular class of bursters and how the dynamics changes with respect to parameters.

Rigorous results related to square-wave bursting are presented in Section 2.3. These results demonstrate that even the simplest models for bursting oscillations lead to very interesting problems associated with the geometric theory of singular perturbations. It need not be true, for example, that the bursting solution is uniquely determined for all ϵ sufficiently small. Moreover, there are multiple ways in which chaotic dynamics may arise as parameters in the model are

varied.

2.2 Bursting Mechanisms

We now describe the mathematical mechanisms responsible for the three classes of bursting oscillations shown in Figure 1. This description follows closely the pioneering work of Rinzel [58]. We only consider the simplest, lowest dimensional models which generate these solutions. As we shall see, square-wave and elliptic bursting can arise in three-dimensional systems, while parabolic bursting requires at least four dimensions. In each case, we consider a system of the form (2.1) and make geometric assumptions concerning the set of fixed points and periodic solutions of (FS). Some assumptions are then needed on the equations governing the slow variables. These assumptions can usually be verified for a specific system by using numerical software.

2.2.1 Square-Wave Bursting

Consider a three-dimensional version of (2.1) of the form

$$\begin{aligned} v' &= f(v,w,y) \\ w' &= g(v,w,y) \\ y' &= \epsilon h(v,w,y,\lambda) \end{aligned} \tag{2.2}$$

A concrete system which exhibits square-wave bursting is given in Remark 2.6. The fast subsystem (FS) now consists of the first two equations in (2.2) with the slow variable y considered as constant. In the third equation, λ represents a fixed parameter. Later, we discuss complex bifurcations that arise when λ is varied.

The primary assumptions on (2.2) concern the bifurcation structure of the fast subsystem with y treated as a parameter. This structure appears in Figure 2, which also shows the projection of the square-wave bursting solution onto the corresponding bifurcation diagram. The set of fixed points of (FS) is assumed to be a Z-shaped curve in the (v,w,y) phase space. We denote this curve by S; only a portion of this Z-shaped curve is shown in Figure 2. The fixed points along the lower branch of S are stable solutions of (FS), while the fixed points on the middle branch of S are saddles. Fixed points along the upper branch of S may be stable or unstable. We also assume that there exists a one-parameter family of periodic solutions of (FS), denoted by P. These limit cycles originate at a (subcritical) Hopf bifurcation along the upper branch of S and terminate along a solution of (FS) that is homoclinic to one of the fixed points on the middle branch of S.

Assumptions are also needed about the slow dynamics. We assume that the y-nullsurface $\{h = 0\}$ defines a two-dimensional manifold that intersects S at a single point. This point lies on the middle branch of S between the homoclinic point and the left knee of S. Finally, $h > 0$ above $\{h = 0\}$ and $h < 0$ below $\{h = 0\}$.

We now give a heuristic explanation for why this system generates a square-wave bursting solution. Suppose that $\epsilon > 0$ is small and consider a solution that begins close to the lower branch. Because this branch consists of stable fixed points of (FS), the trajectory quickly approaches a small neighborhood of the lower branch. The trajectory tracks leftward along the lower branch according to the slow dynamics, until it passes the left knee. This portion of the solution corresponds to the silent phase. Once past the left knee, the trajectory is attracted to near P, the branch of periodic solutions of (FS). This generates the fast repetitive spikes of the bursting solutions. The trajectory passes near P, with increasing y, until it reaches a neighborhood of the homoclinic orbit of (FS). Once it passes the homoclinic orbit, the fast dynamics eventually forces the trajectory back to near the lower branch of S and this completes one cycle of the bursting solution.

This description is formal. It is not at all clear that if the system (2.2) satisfies the above assumptions, then, for all ϵ sufficiently small, there exists a unique periodic solution corresponding to a bursting oscillation. In Section 2.3, we show, in fact, that such a result cannot be true, in general. We describe a result, proved in [46], that the bursting solution will be uniquely determined for all ϵ sufficiently small, except for those ϵ that lie in a certain very small set.

Remark 2.1. A crucial ingredient for square-wave bursting is bistability. This allows for a hysteresis loop between a lower branch of stable fixed points and an upper branch of stable limit cycles. It is also very important that the slow nullsurface $\{h = 0\}$ lies between these two branches. If this last condition is not satisfied, then the system may exhibit other types of solutions. For example, suppose that $\{h = 0\}$ intersects the lower branch of S. This point of intersection will then be a globally stable fixed point of (2.2). If, on the other hand, $\{h = 0\}$ intersects S along its middle branch above the homoclinic point, then (2.2) may give rise to a stable limit cycle which always remains in the active phase near P. This type of solution is referred to as *continuous spiking*. Rigorous results concerning the existence of continuous spiking are presented in [82], [83].

Remark 2.2. Square-wave bursting arises in models for electrical activity in pancreatic β-cells. It is believed that this activity plays an important role in the release of insulin from the cells. The

first mathematical model for this bursting was due to Chay and Keizer [10]. There have been numerous related models, based on experimental data, since then. A review of these models, along with a detailed description of the more biological issues, is given in [67]. Square wave bursting also arises in recent models for respiratory CPG neurons [7] and models for pattern generation based on synaptic depression [81].

Remark 2.3. It is still not clear what underlying biological mechanisms cause bursting oscillations in pancreatic β-cells [15]. In fact, it is possible that bursting may not be generated by the intrinsic properties of a single cell; rather, the bursting may be a network property generated by the coupling between cells. Computational studies in [69] have demonstrated that a population of cells with electrical, or gap-junction, coupling can exhibit bursting oscillations although the parameters of each cell are set so that the cells do not oscillate without any coupling. Detailed analysis of two mutually coupled square-wave bursters is given in [66].

Remark 2.4. Very complicated (global) bifurcations can take place as the parameters ϵ or λ are varied in (2.2). The singular perturbation parameter ϵ controls the rate at which a bursting trajectory passes through the silent and active phases. In particular, the number of spikes per burst is $O(1/\epsilon)$ and becomes unbounded as $\epsilon \to 0$. It is demonstrated in [82] that Smale horseshoe chaotic dynamics can arise during the transition of adding a spike. For example, the solution shown in Figure 3B exhibits a somewhat random variation between 3 and 4 spikes per burst. In Section 2.3, we describe how spikes are added to the bursting solution as ϵ decreases.

Perhaps even more interesting is the bifurcation structure of (2.2) as λ is varied. In the β-cell models, λ is related to the glucose concentration. As the glucose level gradually increases, the cells exhibit resting behavior, then bursting oscillations, and then continuous spiking. This is consistent with behavior exhibited by the model. As λ increases, the y-nullsurface $\{h = 0\}$ intersects the lower branch of S, then the middle branch of S below the homoclinic point, and then the middle branch of S above the homoclinic point. Numerical studies [11] and rigorous analysis [83] have shown that as λ varies between the bursting and continuous spiking regimes, the bifurcation structure of solutions must be very complicated. A Poincaré return map defined by the flow from a section transverse to the homoclinic orbit of (FS) will exhibit Smale-horseshoe dynamics for a robust range of parameter values. This leads to solutions in which the number of spikes per burst varies considerably, as shown in Figure 3A.

Remark 2.5. Some phenomenological, polynomial models for square-wave bursting have been proposed. See, for example, [32], [54], [16]. Analysis of models with two slow variables which

exhibit square-wave bursting is given in [70].

Remark 2.6. A system of equations which give rise to square-wave bursting is [59]:

$$\begin{aligned} v' &= -(g_{ca}m_\infty(v)(v-v_{ca}) + g_k w(v-v_k) + g_l(v-v_l) + g_{kca}z(y)(v-v_k)) + I \\ w' &= 20\phi(w_\infty(v) - w)/\tau(v) \\ y' &= 20\epsilon(-\mu g_{ca}m_\infty(v)(v-v_{ca}) - y) \end{aligned}$$

where, $g_{ca} = 4.$, $g_k = 8.0$, $g_l = 2.0$, $v_k = -84$, $v_l = -60$, $v_{ca} = 120.0$, $I = 45$, $g_{kca} = .25$, $\phi = .23$, $\epsilon = .005$, and $\mu = .02$. The nonlinear functions are given by $m_\infty(v) = .5(1. + \tanh((v + 1.2)/18))$, $w_\infty(v) = .5(1.+\tanh((v-12)/17.4))$, $z(y) = y/(1+y)$ and $\tau(v) = \cosh((v-12.)/34.8)$.

2.2.2 Elliptic Bursting

Elliptic bursting can also arise in a system of the form (2.2) in which there are two fast variables and one slow variable. The bifurcation diagram of (FS) for an elliptic bursting scenario, with the slow variable treated as a parameter, is shown in Figure 4, which includes the projection of the elliptic bursting solution.

Bistability is crucially important for the generation of elliptic bursting, just as it is for square-wave bursting. An important difference, however, is that for elliptic bursting, the curve S of fixed points of (FS) need not be Z-shaped; there may be only one fixed point of (FS) for each value of y. The branch of periodic solutions P now originates at a subcritical Hopf bifurcation along S. To obtain bursting, we hypothesize that the slow variable decreases along S; that is, $h < 0$ near S. During the silent phase, the bursting solution evolves near the stable portion of S until it passes the Hopf point, beyond which the fixed points of S are no longer stable. Note, however, that the trajectory does not jump up to the active phase immediately after crossing the Hopf point. The slow variable y may traverse a distance that is $O(1)$ with respect to ϵ past the Hopf point before jumping up. This type of delayed behavior or slow-passage past a Hopf point has been studied extensively in the singular perturbation literature [53], [2].

We must also hypothesize that there is a net increase in the slow variable as the bursting trajectory passes near P. More precisely, let $(v_y(t), w_y(t))$ denote the periodic solutions along the outer branch of P and suppose that their periods are $T(y)$. Let

$$\bar{h}(y) = \frac{1}{T(y)} \int_0^{T(y)} h(v_y(t), w_y(t), y)dt$$

denote the average of h along these limit cycles. We assume that $\bar{h}(y) > 0$ for each y. Thus during the active phase, y increases until the bursting solution passes the turning point, or knee, of P. The fast dynamics then forces the trajectory back towards S and a new silent phase begins.

Remark 2.7. Both square-wave and elliptic bursting depend on bistability and hysteresis. An important difference between these two classes of bursting is how the active phase terminates. Square-wave bursting ends at a homoclinic bifurcation; the period of oscillation, therefore, increases at the end of each burst. For elliptic bursting, the active phase ends at a saddle node of periodic orbits. There is no pattern for the spike frequencies in general.

Remark 2.8. Elliptic bursting arises in models for thalamic neurons [21], rodent trigeminal neurons [52], and 40-Hz oscillations [48], [92]

Remark 2.9. Here we assumed that the branch of periodic orbits of (FS) originate at a subcritical Hopf bifurcation. Hoppensteadt and Izhikevich [34] show that elliptic bursting is also possible even if the Hopf bifurcation is supercritical.

Remark 2.10. A system of equations which give rise to elliptic bursting is [59]:

$$\begin{aligned} v' &= -(g_{ca}m_\infty(v)(v-v_{ca}) + g_k w(v-v_k) + g_l(v-v_l) + g_{kca}z(y)(v-v_k)) + I \\ w' &= \phi(w_\infty(v) - w)/\tau(v) \\ y' &= \epsilon(-\mu g_{ca}m_\infty(v)(v-v_{ca}) - y) \end{aligned}$$

where, $g_{ca} = 4.4,\ g_k = 8.0,\ g_l = 2.0,\ v_k = -84,\ v_l = -60,\ v_{ca} = 120.0,\ I = 120,\ g_{kca} = .75,\ \phi = 1.2,\ \epsilon = .04$, and $\mu = .016667$. The nonlinear functions are given by $m_\infty(v) = .5(1. + \tanh((v + 1.2)/18))$, $w_\infty(v) = .5(1. + \tanh((v-2.)/30.))$, $z(y) = y/(1+y)$ and $\tau(v) = \cosh((v-2.)/60.)$.

2.2.3 Parabolic Bursting

Both square-wave and elliptic bursting can be achieved in a system with only one slow variable. Moreover, both depend on bistability of the fast dynamics. Parabolic bursting, on the other hand, requires at least two slow variables and does not arise from a hysteresis phenomenon. A geometric model for parabolic bursting is the following. Consider a system of the form (2.1) where $x \in R^2$ and $y = (y_1, y_2) \in R^2$. There are now two slow variables, namely y_1 and y_2. We first describe the bifurcation structure of the fast subsystem with both slow variables considered as parameters. This is illustrated in Figure 5, where we plot one component of the fast variable, corresponding to the membrane potential, along with both slow variables. We also show the projection of a parabolic bursting solution onto this figure.

We hypothesize that the set of fixed points of (FS) forms a Z-shaped surface. The fixed points along the lower branch of this surface are assumed to be stable fixed points of (FS). There is a curve along the upper branch of fixed points where Hopf bifurcations occur. Periodic solutions

arise at these Hopf points and terminate along orbits homoclinic to the fixed points along the lower fold of the fixed point surface. In Figure 5, we show the maximum and minimum values of the fast variable along each of these periodic solutions.

The existence of a parabolic bursting solution also requires hypotheses on the slow dynamics. To write reduced equations which determine the evolution of the slow variables in the silent phase, denote the lower branch of fixed points by $x = \Phi(y)$. The silent phase evolution of the slow variables is then given by the reduced equations

$$\dot{y} = g(\Phi(y), y) \tag{2.3}$$

where differentiation is now with respect to $\tau = \epsilon t$.

One obtains reduced equations for the evolution of the slow variables in the active phase using averaging. Suppose that $y = (y_1, y_2)$ lies in the region where there exists a stable limit cycle of (FS). Let $x_y(t)$ be the corresponding periodic solution of (FS) with period $T(y)$ and consider the averaged quantity

$$\bar{g}(y) \;=\; \frac{1}{T(y)} \int_0^{T(y)} g(x_y(t), y) dt$$

The active phase evolution of the slow variables is then given by the averaged equations

$$\dot{y} = \bar{g}(y) \tag{2.4}$$

Parabolic bursting corresponds to the existence of a closed curve in the slow (y_1, y_2) phase plane which passes through both the region of stable fixed points of (FS), where it satisfies (2.3), and the region of stable limit cycles of (FS), where it satisfies (2.4). This is illustrated in Figure 6.

Note that the active phase of the bursting solution both begins and ends along a curve of homoclinic bifurcations. Since the periods of the limit cycles tend to infinity at the homoclinic bifurcations, the interspike interval is longer at both the beginning and end of each burst. This accounts for the parabolic nature of the period of fast oscillations.

Remark 2.11. Parabolic bursting is found in the Aplysia R-15 neuron [1]. Rinzel and Lee [60] considered a model due to Plant [56] and were the first to give a detailed analysis of parabolic bursting by dissecting the equations into fast and slow subsystems as described here.

Remark 2.12. Rigorous results related to parabolic bursting are given in [43], [73], and [34].

Remark 2.13. A system of equations which give rise to parabolic bursting is [59]:

$$\begin{aligned} v' &= -(i_{ca}(v) + i_k(v) + i_l(v) + i_{kca}(v,c) + i_{cas}(v,s)) + I \\ w' &= \phi(w_\infty(v) - w)/\tau_w(v) \\ c' &= \epsilon(-\mu g_{ca} m_\infty(v)(v - v_{ca}) - c) \\ s' &= \epsilon(s_\infty(v) - s)/\tau_s \end{aligned}$$

where, $i_{ca}(v) = g_{ca} m_\infty(v)(v - v_{ca})$, $i_k(v) = g_k w(v - v_k)$, $i_l(v) = g_l(v - v_l)$, $i_{kca}(v,c) = g_{kca} z(c)(v - v_k)$, and $i_{cas}(v,s) = g_{cas} s(v - v_{ca})$. The constants are given by $g_{ca} = 4.$, $g_k = 8.0$, $g_l = 2.0$, $v_k = -84$, $v_l = -60$, $v_{ca} = 120.0$, $I = 65$, $g_{kca} = 1.$, $\phi = 1.333$, $\epsilon = .002$, $\mu = .025$, $\tau_s = .05$, and $g_{cas} = 1.$. The nonlinear functions are given by $m_\infty(v) = .5(1. + \tanh((v + 1.2)/18))$, $w_\infty(v) = .5(1. + \tanh((v - 12.)/17.))$, $\tau_w(v) = \cosh((v - 12.)/34.)$, $z(c) = c/(1 + c)$, and $s_\infty = .5(1 + \tanh((v - 12/24))$.

2.3 Rigorous Results for Square-Wave Bursting Solutions

Here we present a theorem that addresses the issue of when, and in what sense, the heuristic description of a square-wave bursting trajectory given in Subsection 2.2.1 can be rigorously justified. The theorem implies that there may exist a small range of values of ϵ for which the bursting trajectory is not uniquely determined; moreover, for exactly these values, the bursting solution does not closely follow the heuristically defined orbit. The reason why such values of ϵ exist is related to the mechanism by which spikes are added as ϵ decreases, as we describe here. A more complete discussion is given in [46].

For the following theorem, we consider (2.2) and assume that the geometric assumptions described in Subsection 2.2.1 are satisfied. We also need some technical assumptions concerning the bounded solutions of the fast subsystem (FS). We assume that each of the stable fixed points along the lower branch of S is hyperbolic, the manifold P of periodic solutions is normally hyperbolic, the right knee of S is nondegenerate, and the homoclinic orbit arises from the transverse intersection of stable and unstable manifolds. Finally, we assume that S, P, and orbits heteroclinic to S and P represent all the bounded solutions of (FS).

Theorem 2.1. *The periodic bursting solution is uniquely determined and asymptotically stable for all values of $\epsilon > 0$ sufficiently small except for those in a set of the form $\cup_{i=1}^{\infty} (\epsilon_i - \delta_i, \epsilon_i + \delta_i)$. The ϵ_i and δ_i can be chosen so that $lim_{i\to\infty}\ \epsilon_i = 0$. Moreover,*

$$\epsilon_i - \epsilon_{i+1} > C_1 \epsilon_i^2 \qquad \text{and} \qquad \delta_i \leq C_2 e^{-k/\epsilon_i}$$

for some positive constants C_1, C_2 and k.

The proof of Theorem 2.1 is given in [46]. An important step in the proof is to explain how the bursting solution adds spikes as ϵ varies. It is during these transitions that the heuristic construction is not justified. Here we give a geometric description of how these transitions take place.

The number of spikes is determined by how many times the bursting trajectory spirals around in phase space near P. The active phase terminates when the bursting trajectory passes near the homoclinic orbit of (FS) and jumps down to the lower branch of S. The key to understanding how spikes are added, therefore, is to understand what determines when the trajectory jumps down to the silent phase. As we describe below, this crucially depends on the center-unstable and center-stable manifolds of the fixed points along the middle branch of S. The center-stable manifolds serve to separate those trajectories which continue to spiral in the active phase and those which jump down to the silent phase.

Note that, when $\epsilon = 0$, there are two trajectories in the unstable manifold of each of the fixed points along the middle branch of S. The union of these trajectories forms the center-unstable manifold of the middle branch. One of these trajectories evolves towards the active phase, looping around the upper branch. Suppose that the homoclinic orbit of (FS) is at $y = y_h$. If $y < y_h$, then this trajectory approaches one of the periodic solutions along P, while if $y > y_h$, then it ultimately approaches a stable fixed point along the lower branch. The other unstable trajectory evolves directly towards the silent phase and approaches the stable fixed point along the lower branch. Now the stable manifolds to the fixed points along the middle branch separate the two branches of unstable trajectories. Hence, if a trajectory lies close to the middle branch, it will either give rise to a spike or jump down to the silent phase depending on which side of the appropriate stable manifold it lies on.

What we have described so far holds for $\epsilon = 0$; however, this all carries over for small $\epsilon > 0$. To make this more precise, let W_0^s and W_0^u be the union of all the stable and unstable manifolds to the fixed points along the middle branch when $\epsilon = 0$. (We exclude small neighborhoods of the left and right knees.) These are both smooth, two-dimensional, invariant manifolds. For $\epsilon > 0$, these manifolds perturb to manifolds W_ϵ^s and W_ϵ^u (see [23]), which are also both smooth, two-dimensional, invariant, and lie a C^1-distance $O(\epsilon)$ close to W_0^s and W_0^u near the middle branch. If we let $W_\epsilon^c = W_\epsilon^s \cap W_\epsilon^u$, then W_ϵ^c, W_ϵ^s, and W_ϵ^u are the center, center-stable, and center-unstable manifolds corresponding to the middle branch, respectively. As discussed before, W_ϵ^s divides W_ϵ^u into two pieces; one piece 'points' towards the active phase, while the other piece 'points' towards the silent phase.

We now can see the significance of this separation to bursting solutions. We begin a bursting solution in the active phase near the branch of periodic orbits P. The orbit gives rise to spikes as it tracks near P moving slowly to the right. As the orbit approaches the homoclinic orbit, it passes close to the middle branch. As long as the orbit lies on the 'jump-up' side of W^s_ϵ, it will keep spiking. Once it crosses over to the other side of W^s_ϵ, it will jump down to the silent phase.

It is possible, however, that the orbit lies precisely on W^s_ϵ, and it is important to understand the fate of the trajectory in this case. If the orbit lies on W^s_ϵ, then it must track close to the middle branch (actually W^c_ϵ), slowly moving to the right. The orbit eventually jumps down near the right knee. Note that if we start (exponentially) close to W^s_ϵ, then the trajectory will track close to the middle branch for some finite distance before it either jumps up or jumps down. If the bursting solution behaves in this way, then it will not lie close to the heuristically defined bursting orbit. It is precisely this mechanism (lying close to W^s_ϵ) that can destroy the uniqueness and stability of the bursting solution.

Now consider the transition of adding a spike as ϵ decreases. Suppose, for concreteness, that when $\epsilon = \epsilon_2$, (2.2) exhibits a solution with 2 spikes per burst and when $\epsilon = \epsilon_3$, there are 3 spikes per burst. When $\epsilon = \epsilon_2$, the bursting solution winds around P two times. After the second cycle, it lies on the jump-down side of W^s_ϵ so it falls down to the silent phase. When $\epsilon = \epsilon_3$, however, the bursting solution winds around P three times before jumping down. After two cycles, the solution still lies on the jump-up side of W^s_ϵ, and thus it returns to the active phase. There must exist, therefore, some $\epsilon^* \in (\epsilon_3, \epsilon_2)$ for which a bursting-like solution lies precisely in W^s_ϵ. It is for values of ϵ very close to ϵ^* that the singular construction breaks down.

3 Two Mutually Coupled Cells

3.1 Introduction

In this section, we consider a network consisting simply of two mutually coupled cells. By considering such a simple system, we are relatively easily able to describe how we model networks of oscillators, the types of behavior that can arise in such systems and the mathematical techniques we use for the analysis of the behavior. For this discussion, we assume that each cell, without any coupling, is modeled as the relaxation oscillator

$$\begin{aligned} v' &= f(v,w) \\ w' &= \epsilon g(v,w) \end{aligned} \tag{3.1}$$

Here ϵ is assumed to be small; that is, w represents a slowly evolving quantity. We assume that the $v-$nullcline, $f(v,w) = 0$, defines a cubic-shaped curve and the $w-$nullcline, $g = 0$, is a

monotone decreasing curve which intersects $f = 0$ at a unique point p_0, as shown in Figure 7. We also assume that $f > 0$ ($f < 0$) below (above) the $v-$nullcline and $g > 0$ (< 0) below (above) the $w-$nullcline. If p_0 lies on the middle branch of $f = 0$, then (3.1) gives rise to a periodic solution for all ϵ sufficiently small and we say that the system is *oscillatory*. In the limit $\epsilon \to 0$, one can construct a singular solution as shown in Figure 7. If p_0 lies on the left branch of $f = 0$, then the system is said to be *excitable*; p_0 is a stable fixed point and there are no periodic solutions for all ϵ small.

System (3.1) can be viewed as a simple model for a bursting neuron in which the active phase corresponds to the envelope of a burst's rapid spikes. (See also [42].) Of course, a two-dimensional model for a single cell cannot exhibit the more exotic dynamics described in the previous section for a bursting cell. However, by considering a simple relaxation-type oscillator for each cell, we will be able to discuss how network properties contribute to the emergent behavior of a population of cells. It is, of course, a very interesting issue to understand how this population behavior changes when one considers more detailed models for each cell. Some results for more detailed models are given in [63].

Networks of two coupled cells may display a variety of different rhythms. By a *synchronous* solution, we mean a rhythm in which both cells exhibit exactly the same behavior, oscillating in phase with each other. An *antiphase* solution is shown in Figure 8A. This is the simplest example of what we will call a *clustered* solution. In a larger population of cells, the network is said to exhibit *clustering* if the population breaks up into distinct subgroups such that all of the cells within each subgroup are synchronized with each other, but cells belonging to different subgroups are desynchronized. Figure 8B shows a *suppressed* solution. One of the cells oscillates periodically between the silent and active phases, while the other cell always remains in the silent phase. A more exotic solution is shown in Figure 8C. During each period of oscillation, one of the cells fires two action potentials, while the other cell fires just one.

In the next section, we describe how we model the two mutually coupled cells. The form of coupling used is referred to as *synaptic coupling* and is meant to correspond to a simple model for chemical synapses, the primary means by which neurons in the central nervous system communicate with each other. As we shall see, there are many different forms of synaptic coupling. For example, it may be excitatory or inhibitory and it may exhibit either fast or slow dynamics. We are particularly interested in how the nature of the synaptic coupling affects the emergent population rhythm. A natural question is whether excitatory or inhibitory coupling leads to either synchronous or desynchronous rhythms. There are four possible combinations and

we will demonstrate that all four may be stably realized, depending on the details of the intrinsic and synaptic properties of the cells. Many of the results given here are complementary to those in [42] who use the fast-slow structure in a somewhat different way.

3.2 Synaptic Coupling

We model a pair of mutually coupled neurons by the following system of differential equations

$$\begin{aligned} v_1' &= f(v_1, w_1) - s_2 g_{syn}(v_1 - v_{syn}) \\ w_1' &= \epsilon g(v_1, w_1) \\ v_2' &= f(v_2, w_2) - s_1 g_{syn}(v_2 - v_{syn}) \\ w_2' &= \epsilon g(v_2, w_2) \end{aligned} \tag{3.2}$$

Here (v_1, w_1) and (v_2, w_2) correspond to the two cells. The coupling term $s_j g_{syn}(v_i - v_{syn})$ can be viewed as an additional current which may change a cell's membrane potential v_i. The parameter g_{syn} corresponds to the maximal conductance of the synapse and is positive, while the reversal potential v_{syn} determines whether the synapse is excitatory or inhibitory. If $v < v_{syn}$ along each bounded singular solution, then the synapse is excitatory, while if $v > v_{syn}$ along each bounded singular solution, then the synapse is inhibitory.

The terms s_i, $i = 1, 2$, in (3.2) encode how the postsynaptic conductance depends on the presynaptic potentials v_i. There are several possible choices for the s_i. The simplest choice is to assume that $s_i = H(v_i - \theta_{syn})$, where H is the Heaviside step function and θ_{syn} is a threshold above which one cell can influence the other. Note, for example, that if $v_1 < \theta_{syn}$, then $s_1 = H(v_1 - \theta_{syn}) = 0$, so cell 1 has no influence on cell 2. If, on the other hand, $v_1 > \theta_{syn}$, then $s_1 = 1$ and cell 2 is affected by cell 1.

Another choice for the s_i is to assume that they satisfy a first order equation of the form

$$s_i' = \alpha(1 - s_i)H(v_i - \theta_{syn}) - \beta s_i \tag{3.3}$$

where α and β are positive constants and H and θ_{syn} are as before. Note that α and β are related to the rates at which the synapses turn on or turn off. For *fast synapses*, we assume that both of these constants are $O(1)$ with respect to ϵ. For a *slow synapse*, we assume that $\alpha = O(1)$ and $\beta = O(\epsilon)$; hence, a slow synapse activates on the fast time scale but turns off on the slow time scale.

The synapses considered so far are referred to as *direct* synapses since they are activated as soon as a membrane potential crosses the threshold θ_{syn}. To more fully represent the range of synapse dynamics observed biologically, it is also necessary to consider more complicated

connections. These are referred to as *indirect synapses*, and they are modeled by introducing new dependent variables x_1 and x_2. Each (x_i, s_i) satisfies the equations

$$\begin{aligned} x_i' &= \epsilon\alpha_x(1-x_i)H(v_i-\theta_v) - \epsilon\beta_x x_i \\ s_i' &= \alpha(1-s_i)H(x_i-\theta_x) - \beta s_i \end{aligned} \tag{3.4}$$

The constants α_x and β_x are assumed to be independent of ϵ. The effect of the indirect synapses is to introduce a delay from the time one oscillator jumps up until the time the other oscillator feels the synaptic input. For example, if the first oscillator jumps up, a secondary process is turned on when v_1 crosses the threshold θ_v. The synapse s_1 does not turn on until x_1 crosses θ_x; this takes a finite amount of (slow) time since x_1 evolves on the slow time scale, like the w_i. Note that indirect synapses may be fast or slow. For fast, indirect synapses, the turn off of s_i, after the x_i-induced delay, occurs on the fast time scale.

3.3 Geometric Approach

All of the networks in this paper are analyzed by treating ϵ as a small, singular perturbation parameter. As in the previous section, the first step in the analysis is to identify the fast and slow variables. We then dissect the full system of equations into fast and slow subsystems. The fast subsystem is obtained by simply setting $\epsilon = 0$ in the original equations. This leads to a reduced set of equations for the fast variables with each of the slow variables held constant. The slow subsystems are obtained by first introducing the slow time scale $\tau = \epsilon t$ and then setting $\epsilon = 0$ in the resulting equations. This leads to a reduced system of equations for just the slow variables, after solving for each fast variable in terms of the slow ones. The slow subsystems determine the evolution of the slow variables while the cells are in either the active or the silent phase. During this time, each cell lies on either the left or the right branch of some "cubic" nullcline determined by the total synaptic input which the cell receives. This continues until one of the cells reaches the left or right "knee" of its corresponding cubic. Upon reaching a knee, the cell may either jump up from the silent to the active phase or jump down from the active to the silent phase. The jumping up or down process is governed by the fast equations.

For a concrete example, consider two mutually coupled cells with fast, direct synapses. The dependent variables (v_i, w_i, s_i), $i = 1, 2$, then satisfy (3.2) and (3.3). The slow equations are

$$\begin{aligned} 0 &= f(v_i, w_i) - s_j g_{syn}(v_i - v_{syn}) \\ \dot{w}_i &= g(v_i, w_i) \\ 0 &= \alpha(1-s_i)H(v_i-\theta_{syn}) \; - \; \beta s_i \end{aligned} \tag{3.5}$$

where differentiation is with respect to τ and $i \neq j$. The first equation in (3.5) states that (v_i, w_i) lies on a curve determined by s_j. The third equation states that if cell i is silent ($v_i < \theta_{syn}$), then $s_i = 0$, while if cell i is active, then $s_i = \frac{\alpha}{\alpha+\beta} \equiv s_A$. We demonstrate that it is possible to reduce (3.5) to a single equation for each of the slow variables w_i. Before doing this, it will be convenient to introduce some notation.

Let $\Phi(v, w, s) \equiv f(v, w) - g_{syn} s(v - v_{syn})$. If g_{syn} is not too large, then each $C_s \equiv \{\Phi(v, w, s) = 0\}$ defines a cubic-shaped curve. We express the left and right branches of C_s by $\{v = \Phi_L(w, s)\}$ and $\{v = \Phi_R(w, s)\}$, respectively. Finally, let

$$G_L(w, s) \;=\; g(\Phi_L(w, s), w) \quad \text{and} \quad G_R(w, s) \;=\; g(\Phi_R(w, s), w)$$

Now the first equation in (3.5) can be written as $0 = \Phi(v_i, w_i, s_j)$ with s_j fixed. Hence, $v_i = \Phi_\alpha(v_i, s_j)$ where $\alpha = L$ if cell i is silent and $\alpha = R$ if cell i is active. It then follows that each slow variable w_i satisfies the single equation

$$\dot{w}_i \;=\; G_\alpha(w_i, s_j) \tag{3.6}$$

By dissecting the full system into fast and slow subsystems, we are able to construct singular solutions of (3.2),(3.3). In particular, this leads to sufficient conditions for when there exists a singular synchronous solution and when this solution is (formally) asymptotically stable. The second step in the analysis is to rigorously prove that the formal analysis, in which $\epsilon = 0$, is justified for small $\epsilon > 0$. This raises some very subtle issues in the geometric theory of singular perturbations, some of which have not been completely addressed in the literature. For most of the results presented here, we only consider singular solutions.

We note that the geometric approach used here is somewhat different from that used in many dynamical systems studies (see, for example, [59]). All of the networks considered here consist of many differential equations, especially for larger networks. Traditionally, one would interpret the solution of this system as a single trajectory evolving in a very large dimensional phase space. We consider several trajectories, one corresponding to a single cell, moving around in a much lower dimensional phase space (see also [87], [86], [71], [85], [63]). After reducing the full system to a system for just the slow variables, the dimension of the lower dimensional phase space equals the number of slow intrinsic variables and slow synaptic variables corresponding to each cell. In the worst case considered here, there is only one slow intrinsic variable for each cell and one slow synaptic variable; hence, we never have to consider phase spaces with dimension more than two. Of course, the particular phase space we need to consider may change, depending on whether the cells are active or silent and also depending on the synaptic input that a cell receives.

3.4 Synchrony With Excitatory Synapses

Consider two mutually coupled cells with excitatory synapses. Our goal here is to give sufficient conditions for the existence of a synchronous solution and its stability. Note that if the synapses are excitatory, then the curve $C_A \equiv C_{s_A}$ lies 'above' $C_0 \equiv \{f = 0\}$ as shown in Figure 9. This is because for an excitatory synapse, $v < v_{syn}$ along the synchronous solution. Hence, on C_A, $f(v,w) = g_{syn} s_A (v - v_{syn}) < 0$, and we are assuming that $f < 0$ above C_0. If g_{syn} is not too large, then both C_0 and C_A will be cubic shaped. We assume that the threshold θ_{syn} lies between the two knees of C_0. In the statement of the following result, we denote the left knee of C_0 by (v_{LK}, w_{LK}).

Theorem 3.1. *Assume that each cell, without any coupling, is oscillatory. Moreover, assume the synapses are fast, direct and excitatory. Then there exists a synchronous periodic solution of (3.2), (3.3). This solution is asymptotically stable if one of the following two conditions is satisfied.*

(H1) $\frac{\partial f}{\partial w} < 0, \quad \frac{\partial g}{\partial v} > 0, \quad$ and $\quad \frac{\partial g}{\partial w} < 0$ *near the singular synchronous solution.*

(H2) $|g(v_{LK}, w_{LK})|$ *is sufficiently small.*

Remark 3.1. We note that the synchronous solution cannot exist if the cells are excitable and the other hypotheses, concerning the synapses, are satisfied. This is because along a synchronous solution, each (v_i, w_i) lies on the left branch of C_0 during the silent phase. If the cells are excitable, then each (v_i, w_i) will approach the point where the w-nullcline $\{g = 0\}$ intersects the left branch of C_0. The cells, therefore, will not be able to jump up to the active phase.

Remark 3.2. The assumptions concerning the partial derivatives of f and g in (H1) are not very restrictive since we are already assuming that $f > 0 (< 0)$ below (above) the v-nullcline and $g > 0 (< 0)$ below (above) the w-nullcline.

Remark 3.3. A useful way to interpret (H2) is that the silent phases of the cells are much longer than their active phases. This is because $g(v_{LK}, w_{LK})$ gives the rate at which the slow variables w_i evolve near the end of the silent phase. Note that $g(v_{LK}, w_{LK})$ will be small if the left knee of C_0 is very close to the w-nullcline.

Proof: We first consider the existence of the synchronous solution. This is straightforward because along a synchronous solution $(v_1, w_1, s_1) = (v_2, w_2, s_2) \equiv (v, w, s)$ satisfy the reduced

system

$$\begin{aligned} v' &= f(v,w) - s g_{syn}(v - v_{syn}) \\ w' &= \epsilon g(v,w) \\ s' &= \alpha(1-s)H(v-\theta_{syn}) \ - \ \beta s \end{aligned}$$

The singular solution consists of four pieces. During the silent phase, $s = 0$ and (v, w) lies on the left branch of C_0. During the active phase $s = s_A$ and (v, w) lies on the right branch of C_A. The jumps between these two phases occur at the left and right knees of the corresponding cubics.

We next consider the stability of the synchronous solution to small perturbations. We begin with both cells close to each other in the silent phase on the left branch of C_0, with cell 1 at the left knee ready to jump up. We follow the cells around in phase space by constructing the singular solution until one of the cells returns to the left knee of C_0. As before, the singular solution consists of four pieces. We need to show that the cells are closer to each other after this complete cycle than they were initially.

The first piece of the singular solution begins when cell 1 jumps up. When $v_1(t)$ crosses θ_{syn}, $s_1(t) \to s_A$. This raises the cubic corresponding to cell 2 from C_0 to C_A. If $|w_1(0) - w_2(0)|$ is sufficiently small, corresponding to a sufficiently small perturbation, then cell 2 lies below the left knee of C_A. The fast equations then force cell 2 to also jump up to the active phase, as shown in Figure 9. Note that this piece takes place on the fast time scale. Hence, on the slow time scale, both cells jump up at precisely the same time.

During the second piece of the singular solution, both oscillators lie in the active phase on the right branch of C_A. Note that the ordering in which the oscillators track along the left and right branches has been reversed. While in the silent phase, cell 1 was ahead of cell 2. In the active phase, cell 2 leads the way. The oscillators remain on the right branch of C_A until cell 2 reaches the right knee.

The oscillators then jump down to the silent phase. Cell 2 is the first to jump down. When $v_2(t)$ crosses θ_{syn}, s_2 switches from s_A to 0 on the fast time scale. This lowers the cubic corresponding to cell 1 from C_A to C_0. If, at this time, cell 1 lies above the right knee of C_A, then cell 1 must jump down to the silent phase. This will certainly be the case if the cells are initially close enough to each other.

During the final piece of the singular solution, both oscillators move down the left branch of C_0 until cell 1 reaches the left knee. This completes one full cycle.

To prove that the synchronous solution is stable, we must show that the cells are closer to each other after this cycle; that is, there is compression in the distance between the cells. There

are actually several ways to demonstrate this compression; these correspond to two different ways to define what is meant by the 'distance' between the cells. Here we consider a Euclidean metric, which is defined as follows: Suppose that both cells lie on the same branch of the same cubic and the coordinates of cell i are (v_i, w_i). Then the distance between the cells is defined as simply $|w_1 - w_2|$. Note that during the jump up and the jump down, this metric remains invariant. This is because the jumps are horizontal so the values of w_i do not change. If there is compression, therefore, it must take place as the cells evolve in the silent and active phases. We now show that this is indeed the case if (H1) is satisfied.

Suppose that when $\tau = 0$, both cells lie in the silent phase on C_0. We assume, for convenience, that $w_2(0) > w_1(0)$. We need to prove that $w_2(\tau) - w_1(\tau)$ decreases as long as the cells remain in the silent phase. Now each w_i satisfies (3.6) with $\alpha = L$ and $s_j = 0$. Hence,

$$w_i(\tau) \;=\; w_i(0) \;+\; \int_0^\tau G_L(w_i(\xi), 0) d\xi$$

and, using the Mean Value Theorem,

$$\begin{aligned} w_2(\tau) - w_1(\tau) &= w_2(0) - w_1(0) \;+\; \textstyle\int_0^\tau \; G_L(w_2(\xi), 0) - G_L(w_1(\xi), 0) \; d\xi \\ &= w_2(0) - w_1(0) \;+\; \textstyle\int_0^\tau \; \frac{\partial G_L}{\partial w}(w^*, 0)(w_2(\xi) - w_1(\xi)) \; d\xi \end{aligned} \tag{3.7}$$

for some w^*. Now $G_L(w, s) = g(\Phi_L(w), w)$. Hence, $\frac{\partial G_L}{\partial w} \;=\; g_v \Phi_L'(w) + g_w$. We assume in (H1) that $g_v > 0$ and $g_w < 0$ near the synchronous solution. Moreover, $\Phi_L'(w) < 0$ because $v = \Phi_L(w)$ defines the left branch of the cubic C_0 which has negative slope. It follows that $\frac{\partial G_L}{\partial w} < 0$, and therefore, from (3.7), $w_2(\tau) - w_1(\tau) < w_2(0) - w_1(0)$. This gives the desired compression; a similar computation applies in the active phase. We note that if there exists $\gamma > 0$ such that $\frac{\partial G_L}{\partial w} < -\gamma$ along the left branch, then Gronwall's inequality shows that $w_2(\tau) - w_1(\tau)$ decreases at an exponential rate.

We next consider (H2) and demonstrate why this leads to compression of trajectories. Suppose, for the moment, that $g(v_{LK}, w_{LK}) = 0$; that is, the left knee of C_0 touches the w-nullcline at some fixed point. Then both cells will approach this fixed point as they evolve along the left branch of C_0 in the silent phase. There will then be an infinite amount of compression, since both cells approach the same fixed point. It follows that we can assume that the compression is as large as we please by making $g(v_{LK}, w_{LK})$ sufficiently small. If the compression is sufficiently large, then it will easily dominate any possible expansion over the remainder of the cells' trajectories. This will, in turn, lead to stability of the synchronous solution.

Remark 3.4. The mechanism by which one cell fires, and thereby raises the cubic of the other cell such that it also fires, was referred to as *Fast Threshold Modulation (FTM)* in [71]. There,

a time metric was introduced to establish the compression of trajectories of excitatorily coupled cells, which implies the stability of the synchronous solution. A detailed discussion of the time metric can be found in [42]; see also [49].

Remark 3.5. While the synchronous solution has been shown to be stable, it need not be globally stable. In [45], it is shown that this network may exhibit stable antiphase solutions if certain assumptions on the parameters and nonlinear functions are satisfied.

We have so far considered a completely homogeneous network with just two cells. The analysis generalizes to larger inhomogeneous networks in a straightforward manner, if the degree of heterogeneity between the cells is not too large. The major difference in the analysis is that, with heterogeneity, the cells may lie on different branches of different cubics during the silent and active phases. The resulting solution cannot be perfectly synchronous; however, as demonstrated in [87], one can often expect synchrony in the jump-up, but not in the jump-down. Related work on heterogeneous networks include [72], [55], [8].

One may also consider, for example, an arbitrarily large network of identical oscillators with nearest neighbor coupling. We do not assume that the strength of coupling is homogeneous. Suppose that we begin the network with each cell in the silent phase. If the cells are identical, then they must all lie on the left branch of C_0. Now if one cell jumps up it will excite its neighbors and raise their corresponding cubics. If the cells begin sufficiently close to each other, then these neighbors will jump up due to FTM. In a similar manner, the neighbor's neighbors will also jump due to FTM and so on until every cell jumps up. In this way, every cell jumps up at the same (slow) time. While in the active phase, the cells may receive different input and, therefore, lie on the right branches of different cubics. Once one of the cells jumps down, there is no guarantee that other cells will also jump down at this (slow) time, because the cells to which it is coupled may still receive input from other active cells. Hence, one cannot expect synchrony in the jumping down process. Eventually every cell must jump down. Note that there may be considerable expansion in the distance between the cells in the jumping down process. If $|g(v_{LK}, w_{LK})|$ is sufficiently small, however, as in the previous result, then there will be enough compression in the silent phase so that the cells will still jump up together. Here we assumed that the cells are identical; however, the analysis easily follows if the heterogeneities among the cells are not too large.

3.5 Desynchrony With Inhibitory Synapses

We now consider two mutually coupled cells with inhibitory synapses. Under this coupling, the curve C_A now lies below C_0. As before, we assume that g_{syn} is not too large, such that both C_0 and C_A are cubic shaped. We also assume that the right knee of C_A lies above the left knee of C_0 as shown in Figure 10. Some assumptions on the threshold θ_{syn} are also required. For now, we assume that θ_{syn} lies between the left knee of C_0 and right knee of C_A.

We will assume throughout this section that the synapses are fast, direct and inhibitory. The main results state that if a synchronous solution exists then it must be unstable. The network will typically exhibit either out-of-phase oscillations or a completely quiescent state and we give sufficient conditions for when either of these arises. We note that the network may exhibit bistability; both the out-of-phase and completely quiescent solutions may exist and be stable for the same parameter values. These results are all for singular solutions. Some rigorous results for $\epsilon > 0$ are given in [86].

The first result concerns the existence and stability of the synchronous solution.

Theorem 3.2. *Assume that the synapses are fast, direct and inhibitory. If each cell, without any coupling, is oscillatory and θ_{syn} is sufficiently large, then there exists a singular synchronous solution. This solution is unstable. If each cell, without any coupling, is excitable, then there does not exist a singular synchronous solution.*

Proof: The existence of a singular synchronous solution for oscillatory cells follows precisely as in the previous section. During the silent phase, the trajectory lies on the left branch of C_0, while in the active phase it lies on the right branch of C_A. Note that we require that the right knee of C_A lies above the left knee of C_0. Moreover, when the synchronous solution jumps up and crosses the threshold $v = \theta_{syn}$, it should lie to the right of the middle branch of C_A; otherwise, it would fall down to the silent phase. This is why we assume that θ_{syn} is sufficiently large.

This solution is unstable for the following reason. Suppose both cells are initially very close to each other on C_0. The cells then evolve on C_0 until one of the cells, say cell 1, reaches the left knee of C_0. Cell 1 then jumps up to the active phase. When v_1 crosses the threshold θ_{syn}, s_1 switches from 0 to s_A and cell 2 jumps from C_0 to C_A, as shown in Figure 10. This demonstrates that the cells are uniformly separated for arbitrarily close initial data. The synchronous solution must, therefore, be unstable.

The synchronous solution cannot exist if the cells are excitable for precisely the same reason discussed in the previous section. If such a solution did exist then each cell would lie on C_0

during its silent phase. Each cell would then approach the stable fixed point on this branch and would never be able to jump up to the active phase.

We next consider out-of-phase oscillatory behavior. One interesting feature of mutually coupled networks is that such oscillations can arise even if each cell is excitable for fixed levels of synaptic input. The following theorem gives sufficient conditions for when this occurs. We will require that the active phase of the oscillation is sufficiently long. To give precise conditions, we introduce the following notation.

Assume that the left and right knees of C_0 are at (v_{LK}, w_{LK}) and (v_{RK}, w_{RK}), respectively. If the w-nullcline intersects the left branch of C_A, then we denote this point by $(v_A, w_A) = p_A$. We assume that $w_A < w_{LK}$, as shown in Figure 10. Let τ_L be the (slow) time it takes for the solution of (3.6) with $\alpha = L$ and $s = s_A$ to go from $w = w_{RK}$ to $w = w_{LK}$, and let τ_R be the time it takes for the solution of (3.6) with $\alpha = R$ and $s = 0$ to go from $w = w_{LK}$ to $w = w_{RK}$. Note that τ_L is related to the time a solution spends in the silent phase, while τ_R is related to the time a solution spends in the active phase.

Theorem 3.3. *Assume that the cells are excitable for each fixed level of synaptic input and the synapses are fast, direct, and inhibitory. Moreover, assume that $w_A < w_{LK}$ and $\tau_L < \tau_R$. Then the network exhibits stable out-of-phase oscillatory behavior.*

Remark 3.6. We do not claim that the out-of-phase solution is uniquely determined or that it corresponds to antiphase behavior. These results may hold; however, their proofs require more analysis than that given here.

Remark 3.7. The rest state with each cell at the fixed point on C_0 also exists and is stable. Hence, if the hypotheses of Theorem 3.3 are satisfied, then the network exhibits bistability.

Proof: Suppose that we begin with cell 1 at the right knee of C_0 and cell 2 on the left branch of C_A with $w_A < w_2(0) < w_{LK}$. Then cell 1 jumps down and, when v_1 crosses the threshold θ_{syn}, cell 2's cubic switches from C_A to C_0. Since $w_2(0) < w_{LK}$, cell 2 lies below the left knee of C_0, so it must jump up to the active phase. After these jumps, cell 1 lies on the left branch of C_A, while cell 2 lies on the right branch of C_0.

Cell 2 then moves up the right branch of C_0 while cell 1 moves down the left branch of C_A, approaching p_A. This continues until cell 2 reaches the right knee of C_0 and jumps down. We claim that at this time, cell 1 lies below the left knee of C_0, so it must jump up. We can then keep repeating this argument to obtain the sustained out-of-phase oscillations.

The reason why cell 1 lies below the left knee of C_0 when cell 2 jumps down is because it spends a sufficiently long amount of time in the silent phase. To estimate this time, note that because cell 2 was initially below the left knee of C_0, the time it spends in the active phase before jumping down is greater than τ_R. Hence, the time cell 1 spends in the silent phase from the time it jumps down is greater than $\tau_R > \tau_L$. From the definitions, since cell 1 was initially at the right knee of C_0, it follows that cell 1 must be below the left knee of C_0 when cell 2 jumps down, which is what we wished to show.

Remark 3.8. To obtain sustained oscillations, it is not really necessary to assume that each cell is excitable for all levels of synaptic input. Suppose, for example, that the w-nullcline intersects C_0 along its middle branch, but it intersects C_A along its left branch. Then each cell, without any coupling, is oscillatory. The hypothesis $\tau_L < \tau_R$ is no longer necessary for sustained out-of-phase oscillations. If $\tau_L > \tau_R$, then it is possible that both cells will lie in the silent phase on the left branch of C_0 at the same time. If there is no fixed point of this branch then the leading cell will be able to jump up. At this time, the trailing cell will approach the left branch of C_A and remain there until the leading cell jumps down. The trailing cell may then either jump up, if it lies below the left knee of C_0, or it may jump back to the left branch of C_0. In this latter case, it will eventually jump up when it reaches the left knee of C_0.

Remark 3.9. Wang and Rinzel [95] distinguish between "escape" and "release" in producing out-of-phase oscillations. In the proof of the preceding theorem, the silent cell can only jump up to the active phase once the active cell jumps down and releases the silent cell from inhibition. This is referred to as the release mechanism and is often referred to as *postinhibitory rebound* [24]. To describe the escape mechanism, suppose that each cell is oscillatory for fixed levels of synaptic input. Moreover, one cell is active and the other is inactive. The inactive cell will then be able to escape the silent phase from the left knee of its cubic, despite the inhibition it receives from the active cell. Note that when the silent cell jumps up, it inhibits the active cell. This lowers the cubic of the active cell, so it may be forced to jump down before reaching a right knee. These issues are also discussed in [42], where there is a detailed discussion of properties of the antiphase solutions, including the control of their frequencies.

3.6 Synchrony With Inhibitory Synapses

3.6.1 Introduction

In the previous section, we showed that an inhibitory network cannot exhibit stable synchronous oscillations if the synapses are direct and fast. Synchronous oscillations in an inhibitory network have been observed experimentally, however [77], [79], [98]. We now show that these oscillations are possible with slow and indirect synapses. Recall that the synapse is slow if $\alpha = O(1)$ and $\beta = O(\epsilon)$ with respect to ϵ. We now assume that $\beta = \epsilon K$ where K does not depend on ϵ.

As before, we analyze the network by considering singular solutions. The first step in this analysis is to derive fast and slow equations. This is done in the next subsection. We then show that the synchronous solution may exist with either direct or indirect slow synapses and that this solution cannot be stable if the synapses are direct. In Subsection 3.6.5, we state the main result concerning the stability of the synchronous solution with indirect synapses. This result is proved in [85]. We then demonstrate that mutually coupled networks with slow inhibitory synapses may exhibit numerous other types of solutions besides the synchronous one. In fact, all of the solutions shown in Figure 8 are generated by this class of networks.

3.6.2 Fast and Slow Equations

We derive slow subsystems valid when the cells lie in either the silent or the active phase. There are several cases to consider and we only discuss two of these in detail. Here, we only consider direct synapses; the derivation of the slow equations for indirect synapses is very similar.

If both cells are silent, then $v_i < \theta_{syn}$ and the first term in (3.3) is zero. Hence, after letting $\tau = \epsilon t$ and setting $\epsilon = 0$, (3.2), (3.3) become

$$\begin{aligned} 0 &= f(v_i, w_i) - s_j g_{syn}(v_i - v_{syn}) \\ \dot{w}_i &= g(v_i, w_i) \\ \dot{s}_i &= -K s_i \end{aligned} \tag{3.8}$$

where $j \neq i$. This system can be simplified as follows. We write the left branch of C_s as $v = \Phi_L(w, s)$ and let $G_L(w, s) = g(\Phi_L(w, s), s)$. Each (w_i, s_j) must then satisfy the system

$$\begin{aligned} \dot{w} &= G_L(w, s) \\ \dot{s} &= -K s \end{aligned} \tag{3.9}$$

These equations determine the evolution of the slow equations while in the silent phase.

If both cells are active, then s_i is a fast variable. The only slow variables are the w_i. Instead

of (3.8), the slow equations are now

$$\begin{aligned} 0 &= f(v_i, w_i) - g_{syn}(v_i - v_{syn}) \\ \dot{w}_i &= g(v_i, w_i) \\ 1 &= s_i \end{aligned} \tag{3.10}$$

This can be reduced to a system for just the slow variables as before. Denote the right branch of C_s by $v = \Phi_R(w, s)$ and let $G_R(w, s) = g(\Phi_R(w, s), s)$. Then each w_i satisfies the scalar equation

$$\dot{w} = G_R(w, 1) \tag{3.11}$$

In a similar fashion, we can derive the slow subsystem for when one cell is active and the other is silent. For indirect synapses, there are further cases depending on whether the x_i-variables have crossed their threshold θ_x or not. This is discussed in detail in [85].

3.6.3 Existence of Synchronous Oscillations

The singular synchronous solution is easily constructed; here we consider the case of direct synapses. We begin with both cells at the right knee of the right branch of C_1. From this point, the cells jump down to the silent phase. While in the silent phase, the slow variables evolve according to (3.9). The cells can only leave the silent phase once they reach a left knee of one of the left branches. If the cells are able to reach such a point, then they will jump up to the active phase and return to the starting point. Hence, the existence of the synchronous solution depends on whether the cells can reach one of the jump-up points while in the silent phase.

If the cells are oscillatory, then the synchronous trajectory must reach one of the jump-up points. This is demonstrated in [85], where it is also shown that a synchronous solution can exist even though both cells, without any coupling, are excitable. This will be the case if the rate K of decay of inhibition is small enough and the cells are oscillatory for some fixed values of $s \in (0, 1)$; if the cells are excitable for all $s \in [0, 1]$, then the only stable solution is the quiescent resting state. Exit from the silent phase is not possible if K is too large, since then the inhibition decays quickly and the system behaves in the slow regime like the uncoupled excitable system with $s = 0$.

The construction of the synchronous solution for the case of indirect synapses is very similar. There are some additional complications due to the additional slow variables x_i. The complete analysis is given in [85].

3.6.4 Instability of the Synchronous Solution for Direct Synapses

The synchronous solution is not stable when the synapses are direct for precisely the same reasons described in Section 3.5. This holds because with direct synapses, when one cell jumps, the other cell begins to feel inhibition as soon as the first cell's membrane potential crosses threshold. This instantly moves the second cell away from its threshold by an amount that stays bounded away from zero no matter how close to the first cell the second cell starts. Thus, infinitesimally small perturbations are magnified, at this stage of the dynamics, to finite size, and the synchronous solution cannot be stable.

3.6.5 Statement of the Main Result

We now consider indirect synapses and show that the synchronous solution can be stable in some parameter ranges. We shall show that there are two combinations of parameters that govern the stability. Furthermore, only one of those two combinations controls stability in any one parameter regime.

For this result, it is necessary to make some further assumptions on the nonlinearities and parameters in (3.2), (3.4). It will be necessary to assume that

$$f_w < 0, \quad g_v > 0, \quad \text{and} \quad g_w < 0 \tag{3.12}$$

near the $v-$nullcline. For Theorem 3.4 below, we also assume that $f(v,w)$ is given by

$$f(v,w) = f_1(v) - g_c w(v - v_R)$$

where $g_c > 0$ and $v_R \leq v_{syn}$ represent a maximal conductance and reversal potential, respectively. This holds for the well-known Morris-Lecar equations [51]. The analytical framework we develop, however, also applies to more general nonlinearities which satisfy (3.12). Some technical assumptions are also required on the nonlinear function $g(v,w)$. We need to assume that g_v is not too large near the right branches of the cubics C_s, for example.

We assume that the parameters α_x and β_x are sufficiently large, and $\frac{\alpha_x}{\alpha_x+\beta_x} > \theta_x$. This guarantees that each x_i can cross its threshold in order to turn on the inhibition. Precise conditions on how large α_x and β_x must be are given in [85].

We also need to introduce some notation. Let a_- be defined as the minimum of $-\partial g/\partial w$ over the synchronous solution in the silent phase. Note from (3.12) that $a_- > 0$. Let $(w^*, s^*) = (w_L(s^*), s^*)$ be the point where the synchronous solution meets the jump-up curve, and let $\lambda = w_L'(s^*)$ be the reciprocal slope of the jump-up curve at this point in (w,s)-space. Finally,

let a_+ denote the value of $g(v,w)$ evaluated on the right hand branch of C_0 at the point where the synchronous solution jumps up. The main result is then the following.

Theorem 3.4. *Assume that the nonlinear functions and parameters in (3.2) and (3.4) satisfy the assumptions stated above. If $\beta = \epsilon K$ with $K < a_-$ and $Ks^* < a_+/|\lambda|$, then the synchronous solution is asymptotically stable.*

Remark 3.10. The first condition in Theorem 3.4 is consistent with the numerical simulations of [95], who obtained synchronized solutions when the synapses recovered at a rate slower than the rate at which the neurons recovered in their refractory period.

Remark 3.11. To interpret the second condition in Theorem 3.4, note that Ks^* is the rate of change of s at the point at which the synchronous solution jumps, while a_+ is the rate of change of w on the right hand branch right after the jump. Since $\lambda = dw_L/ds$, multiplication by $|\lambda|$ transforms changes in s to changes to w. Thus, the second condition is analogous to the compression condition that produces synchrony between relaxation oscillators coupled by fast excitation as described in Theorem 3.1 of Section 3.4. $|\lambda|$ may be thought of as giving a relationship between the time constants of inhibitory decay and recovery of the individual cells; a larger $|\lambda|$ (corresponding to a flatter jump-up curve) means that a fixed increment of decay of inhibition (Δs) has a larger effect on the amount of recovery that a cell must undergo before reaching its (inhibition-dependent) threshold for activation.

Remark 3.12. The two conditions given in the statement of Theorem 3.4 correspond to two separate cases considered in the proof of Theorem 3.4. These two cases correspond to whether the two cells preserve their orientation (Case 1) or reverse their orientation (Case 2) on the right branch of the $s = 1$ cubic after one cycle. Theorem 3.4 says that, whatever case the synchronous trajectory falls into, if both conditions hold, then the synchronous solution is stable. Note, however, that the different cases require different conditions. Case 1 requires $K < a_-$ and Case 2 requires $Ks^* < a_+/|\lambda|$. Thus, by changing a parameter, such as g_{syn}, that switches the system between Case 1 and Case 2, one can change which combinations of time scales and other parameters control the stability of the synchronous solution. In particular, stability of synchronous solutions can be lost or gained without changing any time constants. See [85] for details.

Remark 3.13. In this section, we have considered rather simple models for each cell; in particular, each cell contains a single channel state variable w and there is only one intrinsic slow

process. In this case, the synchronous solution can be stable only if the synaptic variable decays on the slow time scale. This is true even if the cells are oscillatory [85], [64]. In fact, if the cells are excitable, then the slow synaptic variable is required even for the existence of a synchronous solution; it allows the cells to escape from the silent phase. In [64], [65], [63], more complicated models for the cells are considered. It is shown that mutually coupled networks with more complex cells can give rise to stable synchronous solutions even if the cells are excitable for all $s \in [0,1]$ and the synapses are fast; the synapses must still be indirect, however. The main conclusion of the analysis in [63] is that what is needed for the existence of stable synchronous solutions is the presence of two slow variables; one of these slow variables may correspond to an intrinsic process and the other to a synaptic process, or both slow variables may correspond to intrinsic processes.

Remark 3.14. The models discussed here represent bursting neurons. Synchronization of spiking neurons, namely neurons with very short active phases, that are connected by inhibition is considered in [90], [25], [6], [42]. We have also assumed that cells and coupling are homogeneous. The effect of heterogeneities on cells coupled with inhibition is analyzed in [26], [97], [12].

3.6.6 Nonsynchronous Solutions

The network of two mutually inhibitory cells can display other behaviors. We will not give rigorous conditions for the existence and stability of these other solutions; instead, we give simulations of the other solutions and a general description of the parameter ranges in which they are expected. The heuristic explanations we give are based on the techniques developed in the previous section. For all of the examples, we consider direct synapses, although the analysis for indirect synapses is very similar.

We start with the antiphase solution. Such a solution is shown in Figure 8A. The antiphase solution is the most well-known solution for a pair of mutually inhibitory oscillators, expected when the inhibition decays at a rate faster than the recovery of the oscillator (K/a_- large); see, for example, [94], [68]. Though K/a_- small favors stability of the synchronous solution and K/a_- large favors the existence of a stable antiphase solution, there is a parameter range in which both solutions are stable.

One can describe the evolution of the antiphase solution in phase space in a way that is similar to the description of the synchronous solution given earlier. In Figure 11, we illustrate the projection of an antiphase solution onto the (w,s) plane. We choose the initial (slow) time so that both cells lie in the silent phase after cell 1 has just jumped down from the active phase.

This implies that the inhibition s_1 felt by cell 2 satisfies $s_1(0) = 1$. Both cells then evolve in the silent phase until cell 2 reaches the jump-up curve, say at time $\tau = \tau_1$. At this time, the inhibition s_2 felt by cell 1 jumps up to the line $s \equiv 1$. Cell 2 then evolves in the active phase; we illustrate the projection of cell 2's trajectory during the active phase with a dotted curve in Figure 11. Note that $s_1(\tau)$ still satisfies $\dot{s}_1 = -Ks_1$; hence, it keeps decreasing while cell 2 is active. During this time, cell 1 lies in the silent phase with $s_2 = 1$. This continues until cell 2 reaches the jump-down curve $w_R(s)$. We denote this time as τ_2. Cell 2 then jumps down and this completes one-half of a complete cycle. For this to be an antiphase solution, we must have that $w_1(\tau_2) = w_2(0)$ and $s_1(\tau_2) = s_2(0)$. Rigorous results related to the existence and stability of antiphase solutions for systems with slow inhibitory coupling are given in [86], [62].

In the introduction to this section, we referred to another kind of nonsynchronous solution obtained in this system as a suppressed solution; an example is shown in Figure 8B. In such rhythms, one cell remains quiet while the other oscillates. They occur in the same parameter range as the stable synchronous solutions, i.e. K/a_- small. The behavior of these solutions is easy to understand: if the inhibition decays slowly enough, the leading cell can recover and burst again before the inhibition from its previous burst wears off enough to allow the other cell to fire. This type of solution cannot exist if the cells are excitable rather than oscillatory, since there is no input from the quiet cell to drive the active one. On the other hand, suppressed solutions only arise if the cells are excitable for some fixed levels of inhibition; i.e. some $s \in (0, 1]$. If this is not the case, then the $w-$coordinate of the suppressed cell must keep decreasing until that cell eventually reaches the jump-up curve and fires.

If the synaptic inhibition decays at a rate comparable to the recovery of the cell, complex hybrid solutions can occur, in which one cell is suppressed for several cycles, while the other fires, and then fires while the other is suppressed. An example is shown in Figure 8C. In this example, each cell is excitable when uncoupled but is oscillatory for some intermediate levels of inhibition. Hence, if K/a_- is sufficiently small, then a cell can fire a number of times while the other cell is suppressed. The inhibition of the firing cell must eventually wear off, such that that cell can no longer fire. This then allows the inhibition of the suppressed cell to wear off to the level from which it can fire. The roles of the two cells are then reversed.

The synchronous solution exists stably in parameter regimes in which one or more of the above nonsynchronous solutions is also stable. Thus the choice of solution depends on the initial condition. The basin of attraction of the synchronous solution depends mainly on the delay of the onset of the inhibition. For a trajectory to be in the domain of attraction of the synchronous

solution, the lagging cell must be activated before the inhibition from the leading cell suppresses it. As the onset time of inhibition decreases, the domain of stability of the synchronous state vanishes, but the nonsynchronous solutions remain.

3.7 Desynchrony With Excitatory Synapses

We now briefly discuss results in [5] which demonstrate that excitatory coupling can lead to *almost synchronous solutions* if the active phase of a single cell is much shorter than the silent phase; that is, the cells here correspond to spiking neurons. This work is motivated by simulations in [55] which showed that there can be a stable state close to synchrony when the fully synchronized state is unstable.

Here we write the equations for a single oscillator as

$$\begin{aligned} v' &= f(v,w) \\ w' &= \epsilon g(v,w)/\tau_\infty(v) \end{aligned} \tag{3.13}$$

where the function $\tau_\infty(v)$ is given by

$$\tau_\infty(v) = \begin{cases} 1 & \text{if } v < v_\theta \\ \epsilon/\gamma & \text{if } v \geq v_\theta \end{cases}$$

The parameter v_θ is the threshold for entering the active phase and γ governs the rate of passage through the active phase. We assume that v_θ lies between the two knees of the cubic $f = 0$, which we again denote by C_0.

The equations for two mutually coupled oscillators in this model are

$$\begin{aligned} v_i' &= f(v_i,w_i) - g_{syn}H(v_j - v_{st})(v_i - v_{syn}) \\ w_i' &= \epsilon g(v_i,w_i)/\tau_\infty(v_i) \end{aligned} \tag{3.14}$$

where $j \neq i$. Here g_{syn} is the conductance of the synaptic current and v_{st} is the synaptic threshold. The synaptic reversal potential v_{syn} is chosen to be high so that the synapse is excitatory; that is, $v_i - v_{syn} < 0$ along the singular solutions. The v-nullcline is the same as that of the uncoupled cell when $v_j < v_{st}$. For $v_j > v_{st}$, the effect of the coupling term is to raise the nullcline and change its shape; if g_{syn} is not too large, then the v-nullcline is still qualitatively cubic. We denote this cubic by C_1. Note that there are two thresholds v_θ and v_{st} in the equations. To simplify the discussion, we assume here that $v_{st} = v_\theta$.

As in previous sections, we analyze the solutions by treating ϵ as a small, singular perturbation parameter. We construct singular solutions after formally setting $\epsilon = 0$. An interesting feature of the model considered here is that the structure of the corresponding flows is quite different depending on whether cells are silent or active.

We first demonstrate how to construct a singular periodic orbit for a single uncoupled cell. When ϵ is set equal to 0 in (3.13), we obtain the equations for the fast flow

$$\begin{aligned} v' &= f(v,w) \\ w' &= 0 \end{aligned} \tag{3.15}$$

if $v < v_\theta$ and

$$\begin{aligned} v' &= f(v,w) \\ w' &= \gamma g(v,w) \end{aligned} \tag{3.16}$$

if $v \geq v_\theta$. By introducing the rescaling $\tau = \epsilon t$ into (3.13) and then setting $\epsilon = 0$, we obtain equations for the slow flow in the silent phase,

$$\begin{aligned} 0 &= f(v,w) \\ \dot{w} &= g(v_L(w),w) \end{aligned} \tag{3.17}$$

if $v < v_\theta$, where $v_L(w)$ is obtained by solving $0 = f(v,w)$ along the left branch of the cubic C_0.

Note that the equations (3.15) and (3.17) are simply scalar equations; in (3.15), the variable w serves as a parameter in the v' equation. The full two-dimensional system (3.13) has been reduced to two one-dimensional equations and solutions of these are easy to characterize. However, (3.16) is not reduced. In other fast-slow systems of the form (3.13), typically the entire v-nullcline consists of rest points for the fast flow. In this case, however, only the portion of C_0 with $v < v_\theta$ consists of rest points.

The singular periodic orbit for a single uncoupled cell is constructed as follows. We begin the orbit with the cell at the left knee of C_0, which we denote by (v_{LK}, w_{LK}). The first part of the singular orbit is a solution of (3.15) which connects (v_{LK}, w_{LK}) and (v_θ, w_{LK}). The second part is a solution of (3.16) which connects (v_θ, w_{LK}) to (v_θ, w_h), where $w_h > w_{LK}$; this corresponds to the active phase. The third part is a solution to (3.15) which connects (v_θ, w_h) back to C_0 at some point $(v_L(w_h), w_h)$. The fourth and final part is a solution to (3.17) which connects $(v_L(w_h), w_h)$ to (v_{LK}, w_{LK}).

The construction of a synchronous solution for the coupled system is done in the same manner as that of the periodic solution for the uncoupled cell; the only difference is that the dynamics are changed as the voltage passes across $v_{st} = v_\theta$. Thus, if each $v_i > v_{st}$, then (3.16) is replaced by

$$\begin{aligned} v' &= f(v,w) - g_{syn}(v - v_{syn}) \\ w' &= \gamma g(v,w) \end{aligned} \tag{3.18}$$

The synchronous solution is not the same as the uncoupled periodic solution, since they satisfy different equations while in the active phase.

There is no difficulty in proving that these singular periodic solutions perturb, for $\epsilon > 0$ small, to actual solutions of either (3.13) or (3.14). See, for example, [50]. The actual periodic orbits for ϵ small lie $O(\epsilon)$ close to the singular orbits, except near the left knee of C_0, where the distance is $O(\epsilon^{1/2})$.

To construct the almost-synchronous solutions, we again work with singular solutions. There are now more cases to consider, depending on which of the cells is silent or active. If both cells are silent (that is, each $v_i < v_\theta$), then the fast flow corresponding to each cell is given by (3.15), while the slow flow is given by (3.17). If both cells are active, then the fast flow for each cell is (3.18); there is no slow flow. Finally, suppose that one of the cells, say cell 1, is active and cell 2 is silent. Then the fast flow for cell 1 is (3.16) and the fast flow for cell 2 is

$$\begin{aligned} v' &= f(v,w) - g_{syn}(v - v_{syn}) \\ w' &= 0 \end{aligned} \tag{3.19}$$

There is no slow flow for this case since all cell 1 dynamics in the active phase occurs on the fast time scale.

We now give a heuristic argument to explain why there may exist a stable almost synchronous solution. We describe the construction of a singular solution of (3.14) in which one of the cells, say cell 1, begins at the left knee of C_0 and cell 2 lies on the left branch of C_0 just above cell 1. We follow the cells around in phase space until one of the cells returns to the left knee. If the other cell returns to the initial position of cell 2, then this will correspond to an almost synchronous solution. As in the previous constructions, the singular solution consists of several pieces.

The first piece starts as cell 1 leaves the left knee; it satisfies (3.15), moving horizontally in (v,w)-space, until it crosses v_θ. Suppose that this occurs when $t = t_1$. At this time, $H(v_1 - v_\theta)$ switches from 0 to 1 and cell 2 then satisfies (3.19). If cell 2 initially lies below the left knee of C_1, then it will jump up, continuing to satisfy (3.19) until v_2 crosses v_θ. Suppose that this occurs when $t = t_2$. For $t_1 < t < t_2$, cell 1 satisfies (3.16). Note that its trajectory is no longer horizontal. We assume in this heuristic argument that $v_1 > v_\theta$ for $t_1 < t < t_2$. When $t = t_2$, $H(v_2 - v_\theta)$ switches from 0 to 1 and both cells then satisfy (3.18). Assume that cell 1 is the first cell to cross v_θ again and this occurs when $t = T_1$. Then cell 2 satisfies (3.16) until it crosses v_θ, say when $t = T_2$. Once a cell crosses v_θ, it moves horizontally to a point on the left branch of C_0. The cells then evolve along the left branch of C_0 until one of the cells returns to the left knee and this completes the cycle. We note that it is possible for either of the cells to be the first to reach the left knee.

The singular flow naturally gives rise to a one-dimensional map, which we denote by Π. More

precisely, if (v_2, w_2) is the initial position of cell 2 on the left branch of C_0 and $(\hat{v}, \hat{w})$ is the position of the trailing cell after the other cell has returned to the left knee, then $\Pi(w_2) = \hat{w}$. This map is well defined if $w_2 - w_{LK}$ is sufficiently small; in particular, this requires that cell 2 initially lies below the left knee of the excited cubic C_1. A fixed point of Π corresponds to a periodic singular almost-synchronous solution. The orbit may be orientation preserving or orientation reversing, depending on whether the first cell to reach the left knee of C_0 is cell 1 or cell 2, respectively. This periodic solution is referred to as an $O(\epsilon)$-synchronous solution for the following reason. The analysis demonstrates that if w_* is the fixed point of Π, then this must lie below the left knee of the excited cubic C_1. Hence, if cell 1 is the first to jump up, then cell 2 will jump up as soon as cell 1 crosses v_θ. The difference between the times the cells reach v_θ is therefore $O(1)$ in t-time. Since the total period in t-time is $O(1/\varepsilon)$, the normalized time difference ($\Delta time/period$) is $O(\varepsilon)$.

We prove the existence of an asymptotically stable fixed point of Π by showing that Π defines a uniform contraction on some interval. We find $\Delta_1 < \Delta_2$ such that Π maps the interval $[\Delta_1, \Delta_2]$ into itself. In particular, $\Pi(\Delta_1) > \Delta_1$ so expansion between cells takes place if they are initially close to each other. This leads to instability of the synchronous solution. The reason why this expansion takes place is because the cells satisfy different equations during their initial times in the active phase. Cell 1 does not feel excitation from cell 2 when it first enters the active phase, so it satisfies (3.16) there. Cell 2, on the other hand, does feel excitation from cell 1 when it enters the active phase, so it satisfies (3.18). Note that in Section 3.4, we proved that the synchronous solution is stable for excitatory synapses if there is slow dynamics in both the silent and active phase. The main difference between the analysis for that system and the one considered here arises during the jumping up process. In Section 3.4, the jump-ups are horizontal and it does not matter that different cells satisfy different fast equations during portions of the jump-ups. Here the jump-ups are not horizontal, so expansion of trajectories can arise.

We conclude by stating two theorems proved in [5]. We will need the following notation. Assume that the right knee of C_1 is at (v_{RK}, w_{RK}) and choose β so that $g(\beta, w_{RK}) = 0$. We say that constants δ_1 and δ_2, which depend on γ, are $O(\gamma)$ apart if there exist K_1 and K_2 such that $K_1\gamma < |\delta_1 - \delta_2| < K_2\gamma$ for γ small.

Theorem 3.5. *Suppose that the constants v_θ and β satisfy one of the following conditions:*

(R) Either $v_\theta > \beta$, or $v_\theta < \beta$ and $\beta - v_\theta$ is sufficiently small.

(P) $v_\theta < \beta$ and g_{syn} is sufficiently small.

Then, for γ sufficiently small, there exist $\Delta_1 < \Delta_2$ such that Π defines a uniform contraction

from the interval $[\Delta_1, \Delta_2]$ *into itself. If* w_* *is the resulting asymptotically stable fixed point of* Π, *then* w_* *and* w_{LK} *are* $O(\gamma)$ *apart. If (P) is satisfied, then* Π *is orientation preserving on* (Δ_1, Δ_2), *while if (R) is satisfied, then* Π *is orientation reversing on* (Δ_1, Δ_2).

Theorem 3.6. *The asymptotically stable singular periodic solution given by Theorem 3.5 perturbs, for* $\epsilon > 0$, *to an asymptotically stable* $O(\epsilon)$*-solution of (3.14).*

4 Globally Inhibitory Networks

4.1 Introduction

We now consider the network illustrated in Figure 12. This is composed of a population of excitatory (E-)cells and a single inhibitory (J-)cell. Each E-cell sends excitation to the J-cell, while the J-cell sends inhibition back to every E-cell. We assume that all of the E-cells are identical, but they may differ from the J-cell. This network, analyzed in [63], [62] is motivated by models for thalamic oscillations involved in sleep rhythms. In those networks, there may be a population of J-cells with inhibitory coupling among the J-cells. This application is explored in Section 5. This type of network was also introduced in [87], [91] as a model for scene segmentation.

We distinguish two types of rhythms in which the network may engage. In a *synchronous oscillation*, the E-cells are completely synchronized. When the E-cells fire, or become active, they excite the J-cell to fire in response. However, the J-cell is not necessarily synchronized with the E-cells throughout the entire oscillation; this is because the J-cell need not have the same intrinsic properties as the E-cells. Alternately, in a *clustered oscillation*, the E-cells form subpopulations or clusters; the cells within a cluster fire synchronously but cells from distinct clusters act out of synchrony from each other. The J-cell will be induced to fire with each cluster.

Two types of solutions for a network with just four E-cells are shown in Figure 13. Figure 13A shows a synchronous solution, while a 2-cluster oscillation is shown in Figure 13B. Note that in each of these figures, the E-cells within a cluster are perfectly synchronized; moreover, the J-cell jumps up together with each cluster. To obtain the different cluster states, as well as a 3-cluster state (not shown), we adjusted a parameter in the equations for the J-cell; this parameter controls the duration of the J-cell's active phase, which, in turn, controls the amount of inhibition sent back to the E-cells. The analysis that follows will clarify why the level of inhibition produced by the J-cell is an important factor in determining the network behavior of the E-cells.

We model the globally inhibitory network as follows (see [63], [62]). Here we assume that all

of the synapses are direct. Each E_i satisfies equations of the form

$$\begin{aligned} v_i' &= f(v_i, w_i) - g_{inh} s_J (v_i - v_{inh}) \\ w_i' &= \epsilon g(v_i, w_i) \\ s_i' &= \alpha(1 - s_i) H(v_i - \theta) - \beta s_i \end{aligned} \tag{4.1}$$

while the J-cell satisfies the equations

$$\begin{aligned} v_J' &= f_J(v_J, w_J) - \tfrac{1}{N} \sum_i s_i g_{exc}(v_J - v_{exc}) \\ w_J' &= \epsilon g_J(v_J, w_J) \\ s_J' &= \alpha_J(1 - s_J) H(v_J - \theta_J) - \epsilon K_J s_J \end{aligned} \tag{4.2}$$

Unlike the previous section, we assume $f > 0$ ($f < 0$) above (below) the v-nullcline for $s_J = 0$ and $g > 0$ ($g < 0$) below (above) the w-nullcline. The nullclines are illustrated in Figure 14. Note that the nullclines are "upside-down" relative to the figures in Section 3. This orientation is motivated by the biological model in Section 5.

The variable s_J denotes the inhibitory synaptic input from the J-cell, while s_i denotes the excitatory synaptic input from cell E_i to the J-cell. The sum in (4.2) is taken over all N E_i-cells. Note that turn on of inhibition and excitation both occur on the fast time scale, while the inhibitory variable s_J turns off on the slow time scale. This turn off may be 'fast' or 'slow', depending on whether K_J is large or small. We assume that $\beta = O(1)$, representing fast turn off of excitation, although there is no problem extending the analysis if $\beta = O(\epsilon)$. Note that if $v_i > \theta$, then $s_i \to s_A \equiv \frac{\alpha}{\alpha+\beta}$ on the fast time scale.

Each synapse in (4.1), (4.2) is direct. If the inhibition is indirect, then s_J satisfies system (3.4), with the appropriate adjustment of subscripts and a new variable x_J included, instead of the equation given in (4.2). Indirect synapses will be necessary to obtain stability of synchronous and clustered solutions to (4.1), (4.2).

As in previous section, we analyze this network by constructing singular solutions. The trajectory for each cell lies on the left (right) branch of a cubic nullcline during the silent (active) phase. Which cubic a cell inhabits depends on the total synaptic input that the cell receives. Nullclines for the E_i are shown in Figure 14A and those for J in Figure 14B. Note in Figure 14A that the $s_J = 1$ nullcline lies above the $s_J = 0$ nullcline, while in Figure 14B, the $s_{tot} \equiv \frac{1}{N}\sum s_i = s_A$ nullcline lies below the $s_{tot} = 0$ nullcline. These relations hold because the E_i receive inhibition from J while J receives excitation from the E_i. We assume that each cell is excitable for fixed levels of synaptic input.

In the next section, we give sufficient conditions, first presented in [63], for when a globally inhibitory network exhibits a stable synchronous solution. Clustered oscillations are considered in

Section 4.3, which follows [62]. Analyzing the stability of clustered solutions entails consideration of two issues, namely what prevents separate clusters from firing together and what maintains the synchrony of the cells belonging to the same cluster. Note that these issues may become especially subtle in cases for which a clustered solution is stable but the completely synchronous state is unstable.

4.2 Synchronous Solution

We now give sufficient conditions for the existence of a singular synchronous periodic solution and for its stability. For existence, we assume that each synapse is direct; there is no problem in extending the analysis to indirect synapses. Indirect synapses are needed for the stability of this solution. To state the main result, it is necessary to introduce some notation. Let C_s denote the cubic $f(v,w) - g_{inh}s(v - v_{inh}) = 0$. Since the E-cells are excitable for fixed levels of the inhibitory input s_J, there is a fixed point on the left branch of C_s of the first two equations in (4.1) with $s = s_J$ held constant. We denote this fixed point by $(v_F(s_J), w_F(s_J))$ and the left knee of C_s by $(v_L(s_J), w_L(s_J))$.

Theorem 4.1. *A singular synchronous periodic solution exists if* $w_F(1) > w_L(0)$, K_J *is sufficiently large, the active phase of the* J*-cell is sufficiently long, and the recovery of the* J*-cell in the silent phase is sufficiently fast. If the inhibitory synapse* s_J *is indirect and the active phase of the* J*-cell is long enough, then the synchronous solution is stable.*

Remark 4.1. The condition $w_F(1) > w_L(0)$ simply states that the fixed point on the left branch of C_1 lies above the left knee of C_0. This allows the possibility of the E-cells firing upon being released from inhibition from the J-cell.

Remark 4.2. Recall that K_J corresponds to the rate of decay of the inhibition. We will see that synchronous oscillations cannot exist if this synaptic decay rate is too slow, given the fact that each E-cell is excitable for fixed levels of synaptic input.

Proof: We prove the existence by demonstrating how to construct the singular synchronous solution if the hypotheses of Theorem 4.1 are satisfied. We assume throughout this construction that the positions of the E-cells are identical. The singular trajectory is shown in Figure 14.

We begin with each cell in the active phase just after it has jumped up. These are the points labeled P_0 and Q_0 in Figure 14. Then each E_i evolves down the right branch of the $s_J = 1$ cubic, while J evolves down the right branch of the $s_{tot} = s_A$ cubic. We assume that the J-cell

active phase is long, such that the E_i have a shorter active phase than J; thus, each E_i reaches the right knee P_1 and jumps down to the point P_2 before J jumps down. The assumption of a long J-cell active phase implies that at this time, J lies above the right knee of the $s_{tot} = 0$ cubic; otherwise, J would jump down as soon as the E_i did. J must therefore jump from the point Q_1 to the point Q_2 along the $s_{tot} = 0$ cubic when the E_i jump down. On the next piece of the solution, J moves down the right branch of the $s_{tot} = 0$ cubic while the E_i move up the left branch of the $s_J = 1$ cubic. When J reaches the right knee Q_3 it jumps down to the point Q_4 on the left branch of the $s_{tot} = 0$ cubic.

Now the inhibition s_J to the E_i starts to turn off on the slow time scale; that is, $\dot{s}_J = -K_J s_J$ for $\dot{} = \frac{d}{d\tau}$, $\tau = \epsilon t$. Thus, the E_i do not jump immediately to another cubic. Instead, the trajectory for the E_i moves upwards, with increasing w_i, until it crosses the w nullcline. Then each w_i starts to decrease. If the E_i are able to reach a left knee, then they jump up to the active phase and this completes one cycle of the synchronous solution. When the E_i jump up, J also jumps up if it lies above the left knee of the $s_{tot} = s_A$ cubic; that is, the recovery of the J-cell in its silent phase must be sufficiently fast.

Existence of the synchronous solution requires that the E-cells can reach the jump-up curve and escape from the silent phase. We demonstrate that this is indeed the case if the assumptions of Theorem 4.1 are satisfied. It will be convenient to first introduce some notation. This will allow us to obtain simple estimates for when a synchronous oscillation exists and what the period of the oscillation is. This notation will also be useful in the next section.

As in earlier sections, we derive equations for the evolution of the E-cells' slow variables; these are (w_i, s_J). Let $v = \Phi_L(w, s)$ denote the left branch of the cubic $f(v, w) - g_{inh} s(v - v_{inh}) = 0$, and let $G_L(w, s) \equiv g(\Phi_L(w, s), s)$. Then each (w_i, s_J) satisfies the slow equations

$$\begin{aligned} \dot{w} &= G_L(w, s_J) \\ \dot{s}_J &= -K_J s_J \end{aligned} \tag{4.3}$$

Figure 15 illustrates the phase plane corresponding to this system. Recall that $w = w_L(s_J)$ denotes the jump-up curve or curve of left knees, and the second curve, which is denoted by $w_F(s_J)$, consists of the fixed points of the first two equations in (4.1) with the input s_J held constant. This corresponds to the w-nullcline of (4.3).

We need to determine when a solution $(w(\tau), s_J(\tau))$ of (4.3), beginning with $s_J(0) = 1$ and $w(0) < w_F(1)$, can reach the jump-up curve $w_L(s_J)$. This is clearly impossible if $w_F(1) < w_L(0)$. If $w_F(1) > w_L(0)$ and $w(0) > w_L(0)$, with K_J sufficiently large, then the solution will certainly reach the jump-up curve; this holds because the solution will be nearly vertical, as shown in

Figure 15. If, on the other hand, K_J is too small, then the solution will never be able to reach the jump-up curve. Instead, the solution will slowly approach the curve $w_F(s_J)$ and lie very close to this curve as s_J approaches zero. This is also shown in Figure 15. We conclude that the cells are able to escape the silent phase if the inhibitory synapses turn off sufficiently quickly and the w-values of the cells are sufficiently large when this turn off begins. Escape is not possible for very slowly deactivating synapses (although it would be possible with slow deactivation if the cells were oscillatory for some levels of synaptic input).

We assume that K_J is large enough so that escape is possible. Choose w_{esc} so that the solution of (4.3) that begins with $s_J(0) = 1$ will be able to reach the jump-up curve if and only if $w(0) > w_{esc}$. The existence of the singular synchronous solution now depends on whether the E_i lie in the region where $w_i > w_{esc}$ when J jumps down to the silent phase. This will be the case if the active phase of J is sufficiently long. One can give a simple estimate on how long this active phase must be as follows.

Let τ_E (τ_J) denote the duration of the E-cell (J-cell) active phase. Further, let w^+ denote the value of w at the right knee of the $s_J = 1$ cubic (see Figure 15). If g_{syn} is not too large, then $w^+ < w_L(0)$. Finally, let τ_{esc} denote the time for w_i to increase from w^+ to w_{esc} under $\dot{w} = G_L(w, 1)$. Since the E_i spend time $\tau_J - \tau_E$ in the silent phase before they are released from inhibition, the singular synchronous solution exists if $\tau_{esc} < \tau_J - \tau_E$.

For the stability of the synchronous solution, we need to assume that s_J corresponds to an indirect synapse, as in Section 3.6. Suppose we slightly perturb the synchronous solution. If s_J is direct, then when one E-cell fires, it will excite the J-cell which will, in turn, inhibit the other E-cells on the fast time scale. This will prevent the other E-cells from firing and desynchrony will result.

The compression of trajectories if s_J is indirect and the J active phase is long enough follows because all the E-cells approach exponentially close to the point $w_F(1)$ in the silent phase while the J-cell is still active. This exponential compression easily dominates any possible expansion over the remainder of the cells' trajectories.

The domain of attraction of the synchronous solution depends on the ability of the E-cells to pass through the 'window of opportunity' provided by the indirect synapse. The size of this domain grows as the J-cell's active phase increases: More powerful J-cell bursts provide increased inhibition to the E-cells and this further compresses the E-cells near the point $w_F(1)$ in the silent phase. We note that this source of compression in globally inhibitory networks is considerably more powerful than any compression mechanism in mutually coupled inhibitory networks.

Remark 4.3. The analysis leads to simple formulas for the period of the synchronous solution. Let τ_J be, as above, the time cell J spends in the active phase and let τ_S be the time for the E-cells to reach the jump up curve after the J-cell jumps down. Then the period of the synchronous solution is simply $\tau_J + \tau_S$. Now τ_J is determined by the dynamics of the J-cell, while τ_S is primarily controlled by the rate at which the synapses turn off; this is the parameter K_J in (4.3). Other parameters play a secondary role. Note, for example, that the parameter g_{syn} mildly influences the period by controlling the slope of the jump up curve.

Remark 4.4. The domain of attraction of the synchronous solution increases with K_J, since a large K_J yields rapid decay of s_J. If K_J is too large, however, then the J-cells actually cannot recover in time to respond to the excitation from the firing E-cells. Hence, this analysis shows that the combination of fast J-cell recovery and a large K_J promotes stable synchronization.

Remark 4.5. An important difference between mutually coupled and globally inhibitory networks arises in the way they use inhibition to synchronize oscillations. In mutually coupled networks with a slow decay of inhibition, the slow decay allows the cells to escape from the silent phase and to come together as they evolve in phase space. In globally inhibitory networks, the J dynamics controls synchronization, and a decay of inhibition on the slow time scale is only needed to allow J-cell recovery.

4.3 Clustered Solutions

4.3.1 Singular Orbit

Here we describe the singular trajectory corresponding to a 2-cluster solution. The number of cells in the network may be arbitrary, but we assume for ease of notation that the clusters have equal numbers of cells. The geometric construction will require certain assumptions on the equations and a precise theorem is stated and proved in the following subsections. As we shall see, the construction of a 2-cluster solution easily generalizes to an arbitrary number of clusters.

For the geometric construction of a singular 2-cluster solution, it suffices to consider only one-half of a complete cycle. During this half-cycle, one cluster, call it E_1, fires, say at $\tau = 0$, and evolves to the initial position of the other cluster; the non-firing cluster, call it E_2, evolves in the silent phase to the initial position of E_1. By symmetry, the solution then continues with the roles of the clusters reversed.

When E_1 jumps up, it forces J to jump up to the right branch of the $s_{tot} = \frac{1}{2}s_A$ cubic. Then E_1 moves down the right branch of the $s_J = 1$ cubic, while J moves down the right branch of the

$s_{tot} = \frac{1}{2}s_A$ cubic and E_2 moves up the left branch of the $s_J = 1$ cubic. We assume, as before, that the E-cells in E_1 have shorter active phases than the J-cell, so E_1 jumps down before J does. The assumption that J has a longer active phase than E_1 implies that it lies above the right knee of the $s_{tot} = 0$ cubic at this time, so it moves down the right branch of the $s_{tot} = 0$ cubic until it reaches the right knee and then jumps down. During the time that J remains active, both E_1 and E_2 move up the left branch of the $s_J = 1$ cubic.

After J jumps down, $s_J(\tau)$ slowly decreases. If E_2 is able to reach the jump-up curve, then it fires and this completes the first half cycle of the singular solution. Suppose that $\tau = \tau_F$ when this occurs. By abuse of notation, let w_i denote the w-value of all cells in cluster E_i. For the trajectories described above to represent one-half of a 2-cluster solution, we need that $w_2(\tau_F) = w_1(0),\ w_1(\tau_F) = w_2(0),$ and $w_J(\tau_F) = w_J(0)$. The analysis in Subsection 4.3.3 shows that a 2-cluster solution will exist, with stability between clusters, if the active phase of J is not too long or too short, compared with the active phase of the E_i. If J's active phase is too long, then the network exhibits synchronous behavior as described before. If J's active phase is too short, then the system approaches the stable quiescent state.

To conclude that the 2-cluster state is stable, we must also consider stability within each cluster. The stability mechanism here is similar to that for a synchronous solution; details are given in Subsection 4.3.4. Since each cluster experiences a decay of inhibition and subsequent re-inhibition between firings, stability within clusters does not require as long a J-cell active phase as does stability of the synchronous solution.

The singular trajectory for an n-cluster oscillation represents a natural generalization of that for the 2-cluster oscillation. In the singular n-cluster solution, if we start when the J-cell falls down, then inhibition to the E-cells decays until one E-cluster fires and causes the J to fire; while these are active, the other $n-1$ E-clusters evolve in the silent phase. The active E-cluster falls down before the J-cell, and the E-clusters then evolve in the silent phase such that each cluster reaches the initial position of the cell ahead of it in the firing sequence at the moment that the J-cell falls down. Precise conditions for the existence and stability of such a solution are given in the next subsection.

4.3.2 Statement of the Main Result

In this subsection, we state our main result concerning the existence and stability of clustered solutions. To clarify the presentation and notation, we will make some simplifying assumptions. A more complete presentation is given in [62]. We begin by discussing the notation that is needed.

While all cells in the network are silent, the E-cell slow variables (w_i, s_J) satisfy (4.3). Let $w_L(s_J)$ and $w_F(s_J)$ be as in the previous section. We assume that $f_w > 0$ near the singular solutions. Since s_J represents inhibitory input, implicit differentiation of the first equation in (4.1) then yields that $w_L'(s_J)$ and $w_F'(s_J)$ are both positive.

As in the previous section, we assume that $w_F(1) > w_L(0)$ and that K_J is sufficiently large to guarantee that escape from the silent phase is possible. Thus, there exists w_{esc} such that the solution of (4.3) beginning at $(w_0, 1)$ will reach the jump-up curve if and only if $w_0 > w_{esc}$. We denote by τ_S the time it takes for this solution to reach the jump-up curve. Note that τ_S depends on the initial position w_0; however, we ignore this dependence here to simplify notation. Otherwise, we could state our results in terms of minimum and maximum times τ_S^{min} and τ_S^{max}. Note also that $w_{esc} \to w_L(0)$ and $\tau_S \to 0$ as $K_J \to \infty$.

Let τ_{esc}, τ_E and τ_J be as in the previous section. Recall that τ_{esc} is the time for w to increase from w^+ to w_{esc} under $\dot{w} = G_L(w, 1)$. Since K_J is large and τ_S is thus small, it follows that the time for w to increase from w^+ to w_{esc}, with several excursions from $s_J = 1$ of duration τ_S, is still approximately τ_{esc}; we use this below but again, a notational adjustment suffices if more precise conditions are desired (see [62]).

Finally, we need to assume that the J cell jumps up if it receives excitation from sufficiently many E cells. Let C_S^J denote the J cell cubic when the J cell receives excitation of strength $s_{tot} = S$. Note that (4.2) has a fixed point on the left branch of C_0^J, call it $w_F^J(0)$. The J can jump up upon receiving excitation of strength S if and only if it lies above the left knee of $w_L^J(S)$ when it is excited. Thus, we assume that there exists M such that if $m \geq M$, then

$$w_L^J(\frac{m}{N} s_A) < w_F^J(0) \tag{4.3}$$

Since we assume that the J cell is active for longer than each E cluster, the J cell jumps down at the right knee of the $s_{tot} = 0$ cubic, call it $w_R^J(0)$. Let $\tau_R(M)$ be the time for the J cell to evolve on the left branch of the $s_{tot} = 0$ cubic from $w_R^J(0)$ to $w_L^J(\frac{M}{N} s_A)$.

With these notation and assumptions, we obtain the following theorem.

Theorem 4.2. *Given N, fix the parameters in (4.1), (4.2) such that the above assumptions are satisfied and assume there exits M such that (4.3) applies for all $m \geq M$. Let n be the unique positive integer such that both of the following hold:*

$$\begin{aligned} i) \quad & n\tau_J - \tau_E + (n-1)\tau_S > \tau_{esc} \\ ii) \quad & (n-1)\tau_J - \tau_E + (n-2)\tau_S < \tau_{esc} \end{aligned}$$

If $n \leq N/M$, $\tau_R(M) < \tau_S$, and K_J is sufficiently large, then there exists an n-cluster periodic solution of (4.1), (4.2) such that each cluster contains at least M cells. This solution is stable, for K_J sufficiently large, if $|G_L(w, s_J)| < |G_R(w, 1)|$ for $w_L(0) < w < w_F(1)$.

Remark 4.6. Theorem 4.2 does not rule out the existence of other stable solutions. In particular, there may be bistability between a clustered solution and the synchronous solution.

Remark 4.7. If $n = 1$, then condition i) becomes $\tau_J > \tau_E + \tau_{esc}$. This is exactly the condition derived before for the existence of a synchronous solution. Here, condition ii) is not relevant. For the 2-cluster case, conditions i), ii) reduce to $\tau_J - \tau_E < \tau_{esc} < 2\tau_J - \tau_E + \tau_S$. In the limit of fast inhibitory decay, $\tau_S \to 0$ and the condition becomes $\frac{1}{2}(\tau_E + \tau_{esc}) < \tau_J < \tau_E + \tau_{esc}$, which was derived in [63].

4.3.3 Idea of the Proof

Theorem 4.2 is proved in [62]. To establish existence, one can select bounds on the distances between clusters such that if all distances start between these bounds, then they stay within these bounds for all time. Condition i) ensures that the leading E cluster can always reach the jump-up curve and fire when its turn arrives, while condition ii) prevents each cluster from catching up to the one ahead of it. As a result, the assumptions of the theorem imply that the E clusters take turns firing, along with the J cell (since $\tau_R(M) < \tau_S$), in such a way that no two clusters are ever simultaneously active. This argument yields a fixed point which is the desired n-cluster periodic solution.

To show the stability of the type of clustered solution considered here, two issues must be addressed. One must show that E-cells within different clusters remain separated from each other; in particular, they can never lie in the active phase at the same time. This actually follows from the existence arguments in [62]. One must also prove that if the E-cells within a cluster are perturbed slightly, then they are compressed under the subsequent flow. This requires indirect inhibition, for the same reasons discussed in Section 3.6. Given that the inhibition is indirect and that $|G_L(w, s_J)| < |G_R(w, 1)|$, stability within clusters follows from compression of E-cells in the jump up after they are released from inhibition. There is no compression or expansion in the jump down because all E-cells jump down from the right knee of the cubic C_1 (see Figure 14).

Remark 4.8. Note that the compression mechanisms responsible for the stability of the synchronous solution and the stability of cells within a cluster for a clustered solution are very

similar. In fact, this compression mechanism is also similar to the compression mechanism in Fast Threshold Modulation, discussed in Section 3.4. In each of these networks, the cells jump up (nearly) horizontally and the slow variable, w, evolves slower before the jump up than after. This produces compression in a time metric (see [42]). What distinguishes these networks is the release mechanism that allows them to jump up. In FTM, one cell reaches the jump-up point at a knee, so that it can *escape* from the silent phase. This, in turn, raises the other cells' cubics so that they are forced to jump up. For the synchronous solution in globally inhibitory networks, all the E-cells jump up after the J-cell falls down and *releases* them from inhibition. In a clustered solution, the cells within one cluster must wait until another cluster jumps down. The J-cell must then still jump down before a new cluster is released from inhibition.

5 Thalamic Sleep Rhythms

Many of the results described in this paper were motivated by models for thalamic oscillations. In particular, recent models for the spindle sleep rhythm [21], [28], [93], [22], [84] resemble the globally inhibitory networks in Section 4. In this section, we describe some of the rhythms generated in the thalamus and a model for them. We then discuss how geometric analysis helps to explain the generation of these rhythms and transitions between them.

5.1 Description of the Sleep Rhythms

In an awake mammal, the thalamus plays an important role in relaying sensory inputs to the appropriate cortical regions. In sleep, neurons in the thalamus engage in rhythms which are believed to interfere with attentiveness to incoming stimuli [78]. During different stages of sleep, different organized forms of thalamic activity arise. For example, drowsiness and shallow sleep are characterized by the *spindle rhythm*, whereas the *delta rhythm* occurs in deeper sleep. Moreover, the spindle rhythm may be transformed into spike-and-wave like epileptiform oscillations, which we may generally classify as paroxysmal discharges [79], [9], [78].

The network that displays the thalamic spindle rhythm falls into the framework of the globally inhibitory networks considered in the previous section. In this network, a population of thalamocortical relay (TC) cells serve as E-cells, sending fast excitation to a population of thalamic reticular (RE) cells, which act as the J-cells in the network. The RE cells send fast ($GABA_A$) and slow ($GABA_B$) inhibition to the TC cells; they also inhibit other RE cells with fast inhibition. The spindle rhythm corresponds to a clustered oscillation in this model. In contrast to the discussion in the previous section, this network has multiple J-cells; however, its clustered

oscillations are qualitatively the same as the type of clustered oscillation discussed there, since the TC cells form separately synchronized clusters which take turns firing while all the RE cells synchronize and fire together in each oscillation.

In experiments, RE-TC networks have been observed to display completely synchronized oscillations in addition to clustering. Synchrony arises, for example, when fast inhibition is removed from the entire network (see [22] and the references therein) or from between the RE cells only [80], [19], [17], [36]. Recent experimental results have also shown that complete synchrony can occur if the RE population receives additional phasic excitation, from cortical input or another source [14], [20], [76], [17]. Hence, the network can change from the clustering of the spindle rhythm to paroxysmal synchrony without any change in thalamic inhibitory synapses.

5.2 A Model For The Spindle Sleep Rhythm

We present the model discussed in [63], which closely resembles that given in [28] (see also [84]). Individual cells are modeled using the Hodgkin-Huxley formalism [33]. Unlike the models in the previous section, two intrinsic slow variables appear in the equations for each cell. As shown in [63], however, the inclusion of additional slow variables in a globally inhibitory network has no significant effect on the synchronization and clustering mechanisms. In the case of synchronization, the strong compression of E-cell trajectories towards a fixed point in the silent phase, afforded by a long J-cell active phase, dominates all other effects with or without this added variable. This contrasts dramatically with the situation for mutually coupled networks, for which the inclusion of an additional slow intrinsic variable significantly impacts escape and synchronization mechanisms.

The following equations include numerous parameters and nonlinearities. These are defined in more detail in [28], [84], [63].

The equations of each TC cell are:

$$\begin{aligned} v_i' &= -I_T(v_i, r_i) - I_{sag}(v_i, h_i) - I_L(v_i) - I_A - I_B \\ r_i' &= (r_\infty(v_i) - r_i)/\tau_r(v_i) \\ h_i' &= (h_\infty(v_i) - h_i)/\tau_h(v_i) \end{aligned} \tag{5.1}$$

Note that the singular perturbation parameter ϵ is absorbed in τ_h, τ_r rather than mentioned explicitly. The terms I_T, I_{sag}, and I_L are intrinsic currents; they are given by: $I_T(v,r) = g_{Ca} m_\infty^2(v) r(v - v_{Ca})$, $I_{sag}(v,h) = g_{sag} h(v - v_{sag})$ and $I_L(v) = g_L(v - v_L)$. Here, g_α and v_α, $\alpha = Ca, sag, L$, correspond to the maximal conductance and reversal potential of each current. Moreover, $m_\infty(v)$ and r correspond to the activation and inactivation variables of the

current I_T, while h corresponds to the activation variable of the current I_{sag}. We note that the cell fires primarily due to the I_T current, corresponding to positively charged Ca^{2+} ions flowing into the cell through calcium channels. For these channels to be open, we need that the I_T current be both activated and deinactivated; this means that both m_∞ and r need to be bounded away from zero. An interesting feature of this model is that deinactivation of the I_T current requires the cell to be hyperpolarized; that is, the membrane potential v must decrease from its resting level. This can be seen from the explicit formula for the nonlinear function $r_\infty(v)$ given in [63]. Hence, a biological explanation for the initiation of TC cell firing is that the inhibition that the TC cells receive from the RE cells hyperpolarizes them which, in turn, deinactivates I_T. This current is also activated at low membrane potentials, which can be seen from the formula for $m_\infty(v)$. Once the calcium channels are open, calcium ions flow into the cell and an action potential is produced.

The terms I_A and I_B represent the fast and slow inhibitory input from the RE cells. We model the fast inhibition I_A as in previous sections; that is, $I_A = g_A(v_i - v_A)\frac{1}{N_{TR}}\sum s_A^j$ where g_A and v_A are the maximal conductance and the reversal potential of the synaptic current. The sum is over all RE cells which make synaptic connections with this TC cell and N_{TR} represents the maximum number of RE cells which send inhibition to a single TC cell. Each synaptic variable s_A^j is direct and satisfies the first order equation

$$s_A^{j\,\prime} = \alpha_R(1 - s_A^j)H(v_R^j - \theta_R) - \beta_R s_A^j \tag{5.2}$$

where v_R^j is the membrane potential variable of the j^{th} RE cell. Motivated by recent experiments [19], [22] , we model the slow inhibition I_B somewhat differently from I_A. We first discuss, however, the model for the RE cells.

The equations of each RE cell are:

$$\begin{aligned} v_R^{i\,\prime} &= -I_{RT}(v_R^i, h_R^i) - I_{AHP}(v_R^i, m_i) - I_{RL}(v_R^i) - I_{RA} - I_E \\ h_R^{i\,\prime} &= (h_{R\infty}(v_R^i) - h_R^i)/\tau_{Rh}(v_R^i) \\ m_i' &= \mu_1[Ca]_i(1 - m_i) - \mu_2 m_i \\ [Ca]_i' &= -\nu I_{RT} - \gamma[Ca]_i \end{aligned} \tag{5.3}$$

The terms I_{RT}, I_{AHP}, and I_{RL} represent intrinsic currents. These are given by $I_{RT}(v,h) = g_{RCa}m_{R\infty}^2(v)h(v - v_{RCa})$, $I_{AHP}(v,m) = g_{AHP}m(v - v_K)$ and $I_{RL}(v) = g_{RL}(v - v_{RL})$. More details concerning the biophysical significance of each term are given in [28], [84].

In (5.3), the term I_{RA} denotes the inhibitory input from other RE cells. It is modeled as $I_{RA} = g_{RA}(v_R^i - v_{RA})\frac{1}{N_{RR}}\sum s_{RA}^j$ where the sum is over all RE cells which make synaptic

connections with the i^{th} RE cell. Each synaptic variable s^j_{RA} satisfies a first order equation similar to (5.2). The term I_E represents excitatory (AMPA) input from the TC cells and is expressed as $I_E = g_E(v^i_R - v_E)\frac{1}{N_{RT}}\sum s^j_E$ where the sum is over all TC cells which make excitatory synaptic connections with the i^{th} RE cell. The synaptic variables s^j_E are fast and also satisfy first order equations similar to (5.2).

It remains to discuss how we model the slow inhibitory current I_B. Similarly to [19], we assume that $I_B = g_B\frac{s^4_{bi}}{s^4_{bi}+\lambda}(v_i - v_B)$ where s_{bi}, along with the variable x_{bi}, satisfies

$$\begin{aligned} s'_{bi} &= k_1 H(x_{bi} - \theta_{xb})(1 - s_{bi}) - k_2 s_{bi} \\ x'_{bi} &= \frac{k_3}{N_{TR}}\left[\sum H(v^i_R - \theta_{Rb})\right](1 - x_{bi}) - k_4 x_{bi} \end{aligned} \tag{5.4}$$

The parameters are such that x_{bi} can only become activated (i.e., exceed θ_{xb}) if a sufficiently large number of RE cells have their membrane potentials v^i_R above the threshold θ_{Rb}. The threshold is chosen rather large so the RE bursts must be sufficiently powerful to activate x_{bi}. Once x_{bi} becomes activated it turns on the synaptic variable s_{bi}; the expression s^4_{bi} in I_B corresponds to synaptic receptor dynamics ([19]) and further delays the effect of the inhibition on the postsynaptic cell.

5.3 Insights From The Geometric Analysis

5.3.1 Removal of Fast Inhibition Promotes Synchronization

The spindle sleep rhythm corresponds to a clustered solution to (5.1)-(5.4). Biologically, RE cells oscillate at about 7-14 Hz in this rhythm; simulations of this model in [63], for example, yielded a frequency of about 12.5 Hz. TC cells, meanwhile, form clusters that each oscillate at a fraction of the spindle frequency, with different TC clusters firing with each RE burst. In this rhythm, fast inhibition from the RE cells to the TC cells and to other RE cells activates with each cycle. Slow inhibition does not activate at all, since the RE cells do not fire powerful enough bursts to keep v^i_R above the threshold θ_{Rb} long enough to activate the variables x_{bi}.

Equations (5.1)-(5.4) also support a synchronous solution, in which all TC and RE cells fire in each cycle, with the RE cells firing almost instantly in response to TC bursts and a frequency of about half that of the clustered oscillation. Experiments and numerical studies have demonstrated that synchrony arises, for example, when fast inhibition is removed from the entire network or from between the RE cells only. The results in the previous section help to clarify why removal of fast inhibition promotes synchronization.

Note that fast inhibition occurs in two places: the RE cells inhibit themselves as well as the TC cells. Removing fast inhibition has different consequences for each of these synaptic

connections and both of these help to synchronize the TC cells (see also [28], [22]). Removing the RE-TC fast inhibition is clearly helpful for synchronization among the TC cells. This holds because the fast inhibition has a very short rise time. This short rise time corresponds to a small window of opportunity for TC firing and a small domain of attraction of the synchronous solution. In fact, it is precisely this inhibition that is responsible for desynchronizing the TC cells during the clustered solution.

Removing the RE-RE fast inhibition appears to be even more crucial for synchronizing the TC cells (see also [80], [35], [19], [17], [36]). This allows the RE cells to fire longer, more powerful bursts which, in turn, activate the slow inhibitory current I_B. The analysis presented for globally inhibitory networks demonstrates that long, powerful bursting of the RE cells is needed for the TC cells to synchronize, unless the desynchronizing effect of inhibition is somehow removed as discussed in [84]. Numerical simulations in [63] show, in fact, that the TC cells will synchronize even if fast inhibition is removed from within the RE population but not from the RE-TC connections.

Why removal of inhibition leads to stronger RE bursts can be easily understood by the analysis of trajectories in phase space. This removal forces the RE cells to lie on the right branch of a different cubic while in the active phase. The cubic of the disinhibited cells lies below the cubic of the cells with inhibition. The disinhibited cells therefore jump up to larger values of membrane potential; moreover, their jump-down point (right knee) lies below the jump down point of the inhibited cells. The disinhibited RE cells, therefore, have a longer active phase.

Note that the slow inhibitory current I_B, activated when RE-RE fast inhibition is removed, has slower rise and decay times than I_A. The slow decay time can help to bring the cells closer together while in the silent phase, as indicated by the results, presented in Section 3.6, on mutually coupled cells with slow inhibition (see also [63]). The slow rise time enhances the domain of attraction of the synchronous solution by expanding the window of opportunity, if the RE-TC fast inhibition is also removed. Hence, both effects improve the ability of the TC cells to synchronize in the absence of fast inhibition, while the former effect may encourage synchrony even if RE-TC fast inhibition remains.

5.3.2 What Determines The Period of Synchronous Oscillations ?

The analysis in Section 4 demonstrates that when TC cells oscillate synchronously, the period of their oscillation equals the time for which the RE cells stay active (τ_J) plus the time it takes for inhibition to decay sufficiently for the next TC firing to occur (τ_S). Thus, only those

parameters that affect these times can influence period. Numerics in [63] verify that increasing the decay rate of inhibition, for example, sharply decreases the period (see also [17]). The rates of change of individual TC cell currents, however, have little effect on period. Geometric analysis of globally inhibitory networks explains this ineffectuality; in a synchronous oscillation, TC cells are compressed close to their silent phase rest state while the RE cells are active, and then the TC cells evolve with little change in their intrinsic currents as inhibition decays. The slow inhibitory conductance g_B also has little effect on τ_J, τ_S and hence on period. The small influence that it does exert comes through its mild influence on the slope of the curve of knees for the TC silent phase, which actually causes a counterintuitive increase in the period as the strength of slow inhibitory coupling increases (see also [93]).

5.3.3 Cortical Inputs Can Enhance Synchronization

Recent papers have emphasized the importance of the cortex in the transformation of spindle oscillations into spike-and-wave-like (SW) epileptiform oscillations in the thalamus [74], [75], [14], [20], [17]. The experiments and modeling described in these works have suggested that this can arise without the removal of fast inhibition from the thalamus. In the network model, one can view the cortex as providing excitatory input to the RE cells. In the mechanism discussed in Subsection 5.3.1, disinhibition of the RE cells leads to more powerful RE bursts and this permits the TC cells to synchronize. The analysis in Section 4 supports the finding [14], [20], [76], [17] that if one does not remove the fast inhibition among the RE cells, but instead induces sufficiently strong excitation from the cortex, then this will have the same effect: the RE cells will fire more powerful bursts, with a longer active phase, because of the additional excitation (their cubics are lowered).

Due to these more powerful bursts, both fast *and* slow inhibition of TC cells ensue, and the resultant additional inhibition implies that TC cells are compressed towards a rest state with larger h, r values. Together with the extended RE active phase, this yields strong compression of TC cells, which combines with the fast decay of fast inhibition to promote TC synchrony, despite the fast rise time of the fast inhibition they receive. In particular, this explains the mechanism behind the results of Destexhe [17], in which sufficiently strong corticothalamic excitation (achieved by blocking only cortical fast inhibition) is found to be crucial for triggering powerful RE bursts. These bursts in turn lead to the activation of fast and slow inhibition in the thalamus and the generation of synchronized ~ 3 Hz oscillations in TC and RE cells.

Acknowledgments. Research for this paper was supported in part by the NSF grants DMS-

9802339 and DMS-9804447.

References

[1] W.B. Adams and J.A. Benson. The generation and modulation of endogenous rhythmicity in the *aplysia* bursting pacemaker neurone R15. *Prog. Biophys. Mol. Biol.*, **46**:1–49, 1985.

[2] S.M. Baer, T. Erneux, and J. Rinzel. The slow passage through a Hopf bifurcation: delay, memory effects, and resonances. *SIAM J. Appl. Math.*, **49**:55–71, 1989.

[3] T. Bal and D. A. McCormick. What stops synchronized thalamocortical oscillations? *Neuron*, **17**:297–308, 1996.

[4] R. Bertram, M.J. Butte, T. Kiemel, and A. Sherman. Topological and phenomenological classification of bursting oscillations. *Bull. Math. Biol.*, **57**:413–439, 1995.

[5] A. Bose, N. Kopell, and D. Terman. Almost-synchronous solutions for networks of neurons coupled by excitation. Submitted.

[6] P. Bush and T. Sejnowski. Inhibition synchronizes sparsely connected cortical neurons within and between columns of realistic network models. *J. Comput. Neurosci.*, pages 91–110, 1996.

[7] R.J. Butera, J. Rinzel, and J.C. Smith. Models of respiratory rhythm generation in the pre-Botzinger complex: I. Bursting pacemaker model. *J. Neurophysiology*, **82**:382–397, 1999.

[8] R.J. Butera, J. Rinzel, and J.C. Smith. Models of respiratory rhythm generation in the pre-Botzinger complex: II. Populations of coupled pacemaker neurons. *J. Neurophysiology*, **82**:398–415, 1999.

[9] G. Buzsáki, R. Llinás, W. Singer, A. Berthoz, and Y. Christen, editors. *Temporal Coding in the Brain.* Springer-Verlag, New York, Berlin, and Heidelberg, 1994.

[10] T.R Chay and J. Keizer. Minimal model for membrane oscillations in the pancreatic β-cell. *Biophys. J.*, **42**:181–190, 1983.

[11] T.R. Chay and J. Rinzel. Bursting, beating, and chaos in an excitable membrane model. *Biophys. J.*, **47**:357–366, 1985.

[12] C. C. Chow. Phaselocking in weakly heterogeneous neuronal networks. *Physica D*, **118**:343–370, 1998.

[13] A.H. Cohen, S. Rossignol, and S. Grillner, editors. *Neural Control of Rhythmic Movements in Vertebrates*. John Wiley and Sons, Inc., New York, 1988.

[14] D. Contreras, A. Destexhe, and M. Steriade. Corical and thalamic participation in the generation of seizures after blockage of inhibition. *Society of Neuroscience Abstracts*, **22**:2099, 1996.

[15] L.D. Cook, L.S. Satin, and W.F. Hopkins. Pancreatic β-cells are bursting, but how? *Trends Neurosci.*, **14**:411–414, 1991.

[16] G. de Vries and R.M. Miura. Analysis of a class of models of bursting electrical activity in pancreatic β-cells. *SIAM J. Appl. Math.*, **58**:607–635, 1998.

[17] A. Destexhe. Spike-and-wave oscillations based on properties of $GABA_B$ receptors. *Journal of Neuroscience*, **18**:9099–9111, 1998.

[18] A. Destexhe, A. Babloyantz, and T. J. Sejnowski. Ionic mechanisms for intrinsic slow oscillations in thalamic relay and reticularis neurons. *Biophys. J.*, **65**:1538–1552, 1993.

[19] A. Destexhe, T. Bal, D. McCormick, and T. Sejnowkski. Ionic mechanisms underlying synchronized oscillations and propagating waves in a model of ferret thalamic slices. *Journal of Neurophysiology*, **76**:2049–2070, 1996.

[20] A. Destexhe, Contreras D, T. J. Sejnowski, and M. Steriade. Cortical projections to the thalamic reticular nucleus may control the spatiotemportal coherence of spindle and epileptic oscillations. *Society of Neuroscience Abstracts*, **22**:2099, 1996.

[21] A. Destexhe, D. A. McCormick, and T. J. Sejnowksi. A model for 8-10 Hz spindling in interconnected thalamic relay and reticularis neurons. *Biophys. J.*, **65**:2474–2478, 1993.

[22] A. Destexhe and T. Sejnowski. Synchronized oscillations in thalamic networks: insights from modeling studies. In M. Steriade, E. Jones, and D. McCormick, editors, *Thalamus, Volume II*, pages 331–372. Elsevier, Amsterdam, 1997.

[23] N. Fenichel. Geometric singular perturbation theory. *J. Differ. Equations*, **31**:53–91, 1979.

[24] W. Friesen. Reciprocal inhibition, a mechanism underlying oscillatory animal movements. *Neurosci. Behavior*, **18**:547–553, 1994.

[25] W. Gerstner, J. L. van Hemmen, and J. Cowan. What matters in neuronal locking? *Neural Comput.*, **8**:1653–1676, 1996.

[26] D. Golomb and J. Rinzel. Dynamics of globally coupled inhibitory neurons with heterogeneity. *Physical Review E*, **48**:4810–4814, 1993.

[27] D. Golomb and J. Rinzel. Clustering in globally coupled inhibitory neurons. *Physica D*, **72**:259–282, 1994.

[28] D. Golomb, X.-J. Wang, and J. Rinzel. Synchronization properties of spindle oscillations in a thalamic reticular nucleus model. *J. Neurophysiol.*, **72**:1109–1126, 1994.

[29] D. Golomb, X.-J. Wang, and J. Rinzel. Propagation of spindle waves in a thalamic slice model. *Journal of Neurophysiology*, **75**:750–769, 1996.

[30] C.M. Gray. Synchronous oscillations in neuronal systems: Mechanisms and functions. *J. Comput. Neurosci.*, **1**:11–38, 1994.

[31] C.M. Gray and D.A. McCormick. Chattering cells: Superficial pyramidal neurons contributing to the generation of synchronous oscillations in the visual cortex. *Science*, **274**:109–113, 1996.

[32] J.L Hindmarsh and R.M. Rose. A model of neuronal bursting using three coupled first order differential equations. *Proc. R. Soc. Lond., Ser. B*, **221**:87–102, 1984.

[33] A.L. Hodgkin and A.F. Huxley. A quantitative description of membrane current and its application to conduction and excitation in a nerve. *Journal of Physiology*, **117**:165–181, 1952.

[34] F.C. Hoppensteadt and E.M. Izhikevich. *Weakly Connected Neural Networks*. Springer-Verlag, New York, Berlin, and Heidelberg, 1997.

[35] J. Huguenard and D. Prince. Clonazepam suppresses $GABA_b$-mediated inhibition in thalamic relay neurons through effects in nucleus reticularis. *Journal of Neurophysiology*, **71**:2576–2581, 1994.

[36] M. Huntsman, D. Porcello, G. Homanics, T. DeLorey, and J. Huguenard. Reciprocal inhibitoryu connections and network synchrony in the mammalian thalamus. *Science*, **283**:541–543, 1999.

[37] E.M. Izhikevich. Neural excitability, spiking, and bursting. *International Journal of Bifurcation and Chaos*, **10**, 2000.

[38] J.W. Jacklet, editor. *Neuronal and Cellular Oscillators*. Marcel Dekker Inc, New York, 1989.

[39] J.G.R. Jeffreys, R.D. Traub, and M. A. Whittington. Neuronal networks for induced '40 Hz' rhythms. *Trends Neurosci.*, **19**:202–207, 1996.

[40] E.R. Kandel, J.H. Schwartz, and T.M. Jessell. *Principles of Neural Science*. Appleton & Lange, Norwalk, Conn., 1991.

[41] U. Kim, T. Bal, and D. A. McCormick. Spindle waves are propagating synchronized oscillations in the ferret LGNd in vitro. *Journal of Neurophysiology*, **74**:1301–1323, 1995.

[42] N. Kopell and B. Ermentrout. Mechanisms of phase-locking and frequency control in pairs of coupled neural oscillators. In B. Fiedler, G. Iooss, and N. Kopell, editors, *Handbook of Dynamical Systems, vol. 3: Towards Applications*. Elsevier. To appear.

[43] N. Kopell and G.B. Ermentrout. Subcellular oscillations and bursting. *Math. Biosci.*, **78**:265–291, 1986.

[44] N. Kopell and G. LeMasson. Rhythmogenesis, amplitude modulation and multiplexing in a cortical architecture. *Proc. Natl. Acad. Sci. USA*, **91**:10586–10590, 1994.

[45] N. Kopell and D. Somers. Anti-phase solutions in relaxation oscillators coupled through excitatory synapses. *J. Math. Biol.*, **33**:261–280, 1995.

[46] E. Lee and D. Terman. Uniqueness and stability of periodic bursting solutions. *Journal of Differential Equations*. To appear.

[47] R. R. Llinás. The intrinsic electrophysiological properties of mammalian neurons: Insights into central nervous system function. *Science*, **242**:1654–1664, 1988.

[48] R.R. Llinas, T. Grace, and Y. Yarom. *In vitro* neurons in mammalian cortical layer 4 exhibit intrinsic oscillatory activity in the 10- to 50 Hz frequency range. *Proc. Natl. Acad. Sci. USA*, **88**:897–901, 1991.

[49] T. LoFaro and N. Kopell. Timing regulation in a network reduced from voltage-gated equations to a one-dimensional map. *J. Math. Biol.* To appear.

[50] E.F. Mischenko and N.Kh. Rozov. *Differential Equations with Small Parameters and Relaxation Oscillations.* Plenum Press, New York and London, 1975.

[51] C. Morris and H. Lecar. Voltage oscillations in the barnicle giant muscle fiber. *Biophys. J.*, **35**:193–213, 1981.

[52] C.A. Del Negro, C.-F. Hsiao, S.H. Chandler, and A. Garfinkel. Evidence for a novel bursting mechanism in rodent trigeminal neurons. *Biophys. J.*, **75**:174–182, 1998.

[53] A. Nejshtadt. Asymptotic investigation of the loss of stability by an equilibrium as a pair of eigenvalues slowly cross the imaginary axis. *Usp. Mat. Nauk*, **40**:190–191, 1985.

[54] M. Pernarowski. Fast subsystem bifurcations in a slowly varying Lienard system exhibiting bursting. *SIAM J. Appl. Math.*, **54**:814–832, 1994.

[55] P. Pinsky and J. Rinzel. Intrinsic and network rhythmogenesis in a reduced Traub model for CA3 neurons. *J. Comput. Neurosci.*, **1**:39–60, 1994.

[56] R.E. Plant. Bifurcation and resonance in a model for bursting nerve cells. *J. Math. Biol.*, **11**:15–32, 1981.

[57] J. Rinzel. Bursting oscillations in an excitable membrane model. In B.D. Sleeman and R.J. Jarvis, editors, *Ordinary and Partial Differential Equations.* Springer-Verlag, New York, 1985.

[58] J. Rinzel. A formal classification of bursting mechanisms in excitable systems. In A.M. Gleason, editor, *Proceedings of the International Congress of Mathematicians*, pages 1578–1594. American Mathematical Society, Providence, RI, 1987.

[59] J. Rinzel and G.B. Ermentrout. Analysis of neural excitability and oscillations. In C.Koch and I. Segev, editors, *Methods in Neuronal Modeling: From Ions to Networks*, pages 251–291. The MIT Press, Cambridge, MA, second edition, 1998.

[60] J. Rinzel and Y.S. Lee. Dissection of a model for neuronal parabolic bursting. *J. Math. Biol.*, **25**:653–657, 1987.

[61] J. Rinzel, D. Terman, X.-J. Wang, and B. Ermentrout. Propagating activity patterns in large-scale inhiitory neuronal networks. *Science*, **279**:1351–1355, 1998.

[62] J. Rubin and D. Terman. Analysis of clustered firing patterns in synaptically coupled networks of oscillators. Submitted.

[63] J. Rubin and D. Terman. Geometric analysis of population rhythms in synaptically coupled neuronal networks. *Neural Comput.* To appear.

[64] J. Rubin and D. Terman. Geometric analysis of population rhythms in synaptically coupled neuronal networks. *IMA Preprint Series # 1586*, 1998.

[65] J. Rubin and D. Terman. Geometric analysis of neuronal firing patterns in network models with fast inhibitory synapses. *Neurocomputing*, **26-27**:491–498, 1999.

[66] A. Sherman. Anti-phase, asymmetric and aperiodic oscillations in excitable cells – I. coupled bursters. *Bull. Math. Biol.*, **56**:811–835, 1994.

[67] A. Sherman. Contributions of modeling to understanding stimulus-secretion coupling in pancreatic β-cells. *American. J. Phyciology*, **271**:547–559, 1996.

[68] F. Skinner, N. Kopell, and E. Marder. Mechanisms for oscillation and frequency control in networks of mutually inhibitory relaxation oscillators. *J. Comput. Neurosci.*, **1**:69–87, 1994.

[69] P. Smolen, J. Rinzel, and A. Sherman. Why pancreatic islets burst but single β-cells do not: The heterogeneity hypothesis. *Biophys. J.*, **64**:1668–1680, 1993.

[70] P. Smolen, D. Terman, and J. Rinzel. Properties of a bursting model with two slow inhibitory variables. *SIAM J. Appl. Math.*, **53**:861–892, 1993.

[71] D. Somers and N. Kopell. Rapid synchronization through fast threshold modulation. *Biol. Cybern.*, **68**:393–407, 1993.

[72] D. Somers and N. Kopell. Waves and synchrony in networks of oscillators of relaxation and non- relaxation type. *Physica D*, **89**:169–183, 1995.

[73] C. Soto-Trevino, N. Kopell, and D. Watson. Parabolic bursting revisited. *J. Math. Biol.*, **35**:114–128, 1996.

[74] M. Steriade. Coherent activities in corticothalamic networks during resting sleep and their development into paroxysmal events. In G. Buzsáki, R. Llinás, W. Singer, A. Berthoz, and Y. Christen, editors, *Temporal Coding in the Brain.* Springer-Verlag, 1994.

[75] M. Steriade, D. Contreras, and F. Amzica. Synchronized sleep oscillations and their paroxysmal developments. *Trends Neurosci.*, **17**:199–208, 1994.

[76] M. Steriade, D. Contreras, and F. Amzica. The thalamocortical dialogue during wake, sleep, and paroxysmal oscillations. In M. Steriade, E. Jones, and D. McCormick, editors, *Thalamus, Volume II*, pages 213–294. Elsevier, Amsterdam, 1997.

[77] M. Steriade, L. Domich, G. Oakson, and M. Deschênes. Abolition of spindle oscillations in thalamic neurons disconnected from nucleus reticularis thalami. *Journal of Neurophysiology*, **57**:260–273, 1987.

[78] M. Steriade, E. Jones, and D. McCormick, editors. *Thalamus, Volume II.* Elsevier, Amsterdam, 1997.

[79] M. Steriade, E. G. Jones, and R. R. Llinás. *Thalamic Oscillations and Signaling.* Wiley, New York, 1990.

[80] M. Steriade, D.A. McCormick, and T.J. Sejnowski. Thalamocortical oscillations in the sleep and aroused brain. *Science*, **262**:679–685, 1993.

[81] J. Tabak, W. Senn, M.J. O'Donovan, and J. Rinzel. Comparison of two models for pattern generation based on synaptic depression. *Neurocomputing*, **26-27**:551–556, 1999.

[82] D. Terman. Chaotic spikes arising from a model for bursting in excitable membranes. *SIAM J. Appl. Math.*, **51**:1418–1450, 1991.

[83] D. Terman. The transition from bursting to continuous spiking in an excitable membrane model. *J. Nonlinear Sci.*, **2**:133–182, 1992.

[84] D. Terman, A. Bose, and N. Kopell. Functional reorganization in thalamocortical networks: Transition between spindling and delta sleep rhythms. *Proc. Natl. Acad. Sci. USA*, **93**:15417–15422, 1996.

[85] D. Terman, N. Kopell, and A. Bose. Dynamics of two mutually coupled inhibitory neurons. *Physica D*, **117**:241–275, 1998.

[86] D. Terman and E. Lee. Partial synchronization in a network of neural oscillators. *SIAM J. Appl. Math.*, **57**:252–293, 1997.

[87] D. Terman and D. L. Wang. Global competition and local cooperation in a network of neural oscillators. *Physica D*, **81**:148–176, 1995.

[88] D.H. Terman, G.B. Ermentrout, and A.C. Yew. Geometric singular perturbation analysis of wave propagation in thalamic networks. Preprint.

[89] R. D. Traub and R. Miles. *Neuronal Networks of the Hippocampus*. Cambridge University Press, New York, 1991.

[90] C. van Vreeswijk, L. Abbott, and G. B. Ermentrout. When inhibition, not excitation, synchronizes neural firing. *J. Comput. Neurosci.*, **1**:313–321, 1994.

[91] D.L. Wang and D. Terman. Locally excitatory globally inhibitory oscillator networks. *IIIE Trans. Neural Nets*, **6**:283–286, 1995.

[92] X.-J. Wang. Ionic basis for intrinsic-40 Hz neuronal oscillations. *Neuroreport*, **5**:221–224, 1993.

[93] X.-J. Wang, D. Golomb, and J. Rinzel. Emergent spindle oscillations and intermittent burst firing in a thalamic model: specific neuronal mechanisms. *Proc. Natl. Acad. Sci. USA*, **92**:5577–5581, 1995.

[94] X.-J. Wang and J. Rinzel. Alternating and synchronous rhythms in reciprocally inhibitory model neurons. *Neural Comput.*, **4**:84–97, 1992.

[95] X.-J. Wang and J. Rinzel. Spindle rhythmicity in the reticularis thalamic nucleus: synchronization among mutually inhibitory neurons. *Neuroscience*, **53**:899–904, 1993.

[96] X.-J. Wang and J. Rinzel. Oscillatory and bursting properties of neurons. In M.A. Arbib, editor, *The Handbook of Brain Theory and Neural Networks*, pages 686–691. The MIT Press, Cambridge, London, 1995.

[97] J. White, C. C. Chow, J. Ritt, C. Soto, and N. Kopell. Synchronization and oscillatory dynamics in heterogeneous, mutually inhibited neurons. *J. Comput. Neurosci.*, **5**:5–16, 1998.

[98] M. A. Whittington, R. D. Traub, and J. G. R. Jeffreys. Synchronized oscillations in interneuron networks driven by metabotropic glutamate receptor activation. *Nature*, **373**:612–615, 1995.

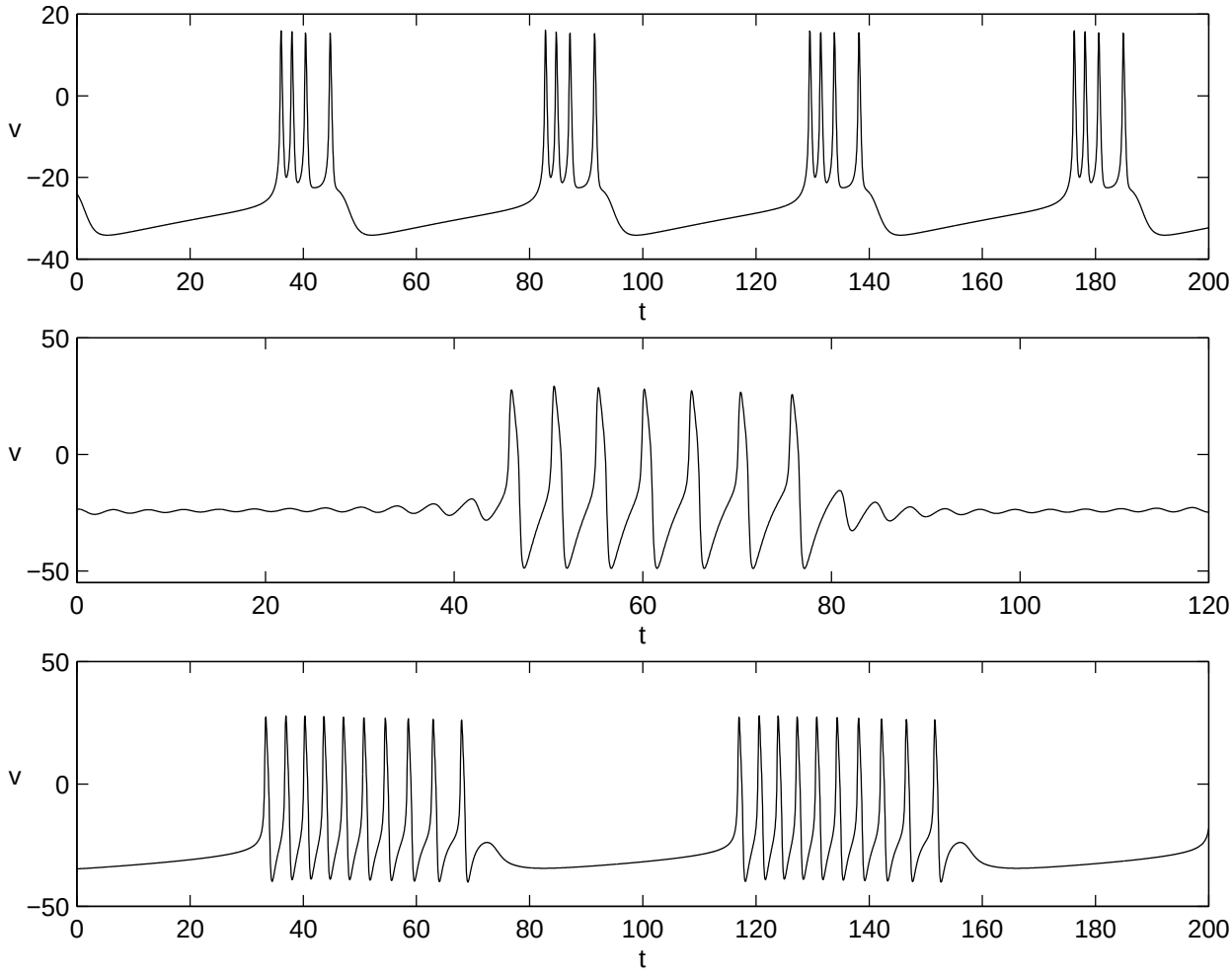

Figure 1: Classes of bursting oscillations. A. (top) Square-wave bursting. B. (middle) Elliptic bursting. C. (bottom) Parabolic bursting.

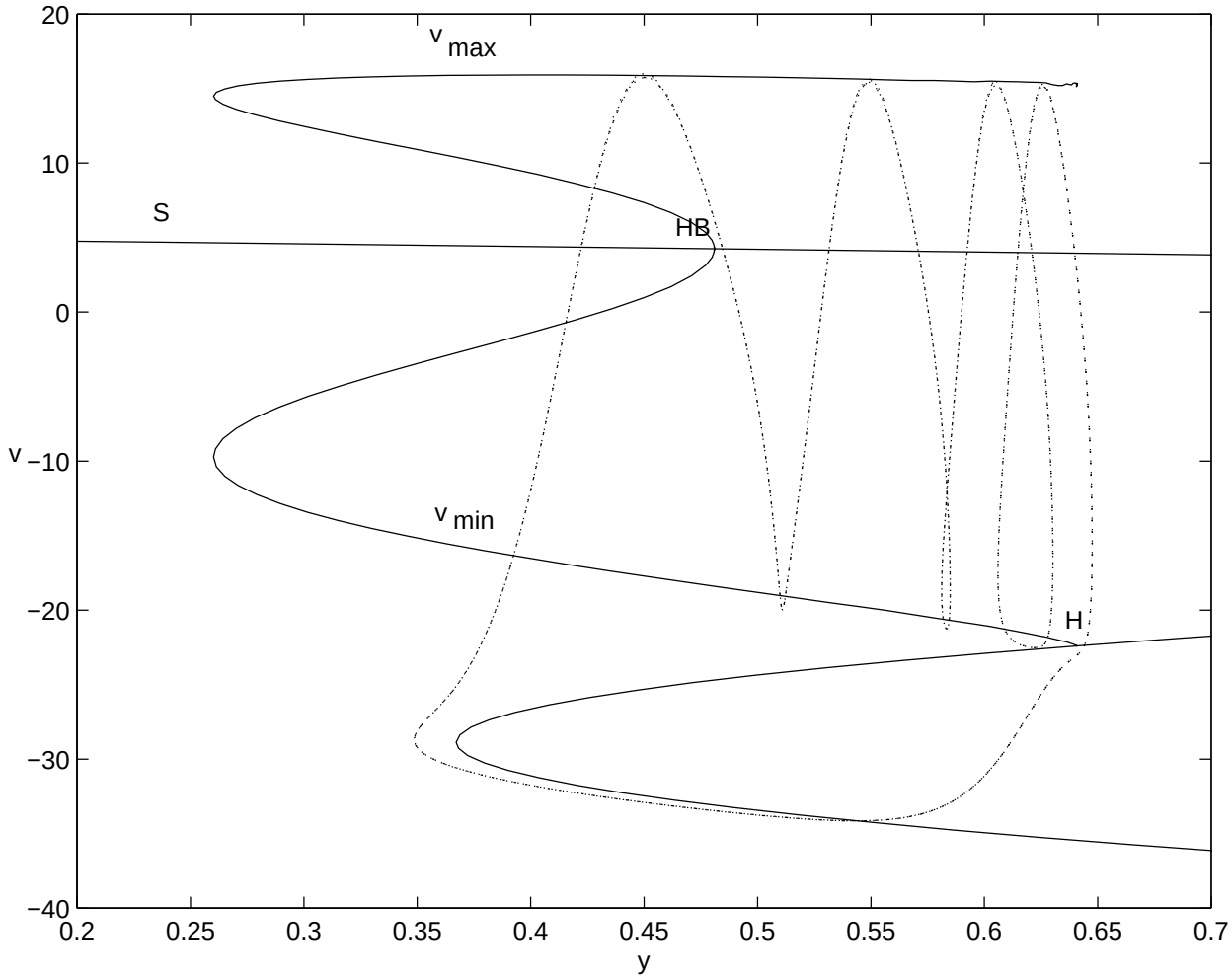

Figure 2: Bifurcation structure for square-wave bursting. Here, v_{max}, v_{min} denote maximum and minimum values achieved by the stable periodic orbits of (FS). S consists of fixed points of (FS) and continues in the lower right of the figure, where the left knee appears. Homoclinic and Hopf bifurcations occur at H and HB, respectively. The dotted trajectory is the projection of a square-wave bursting solution.

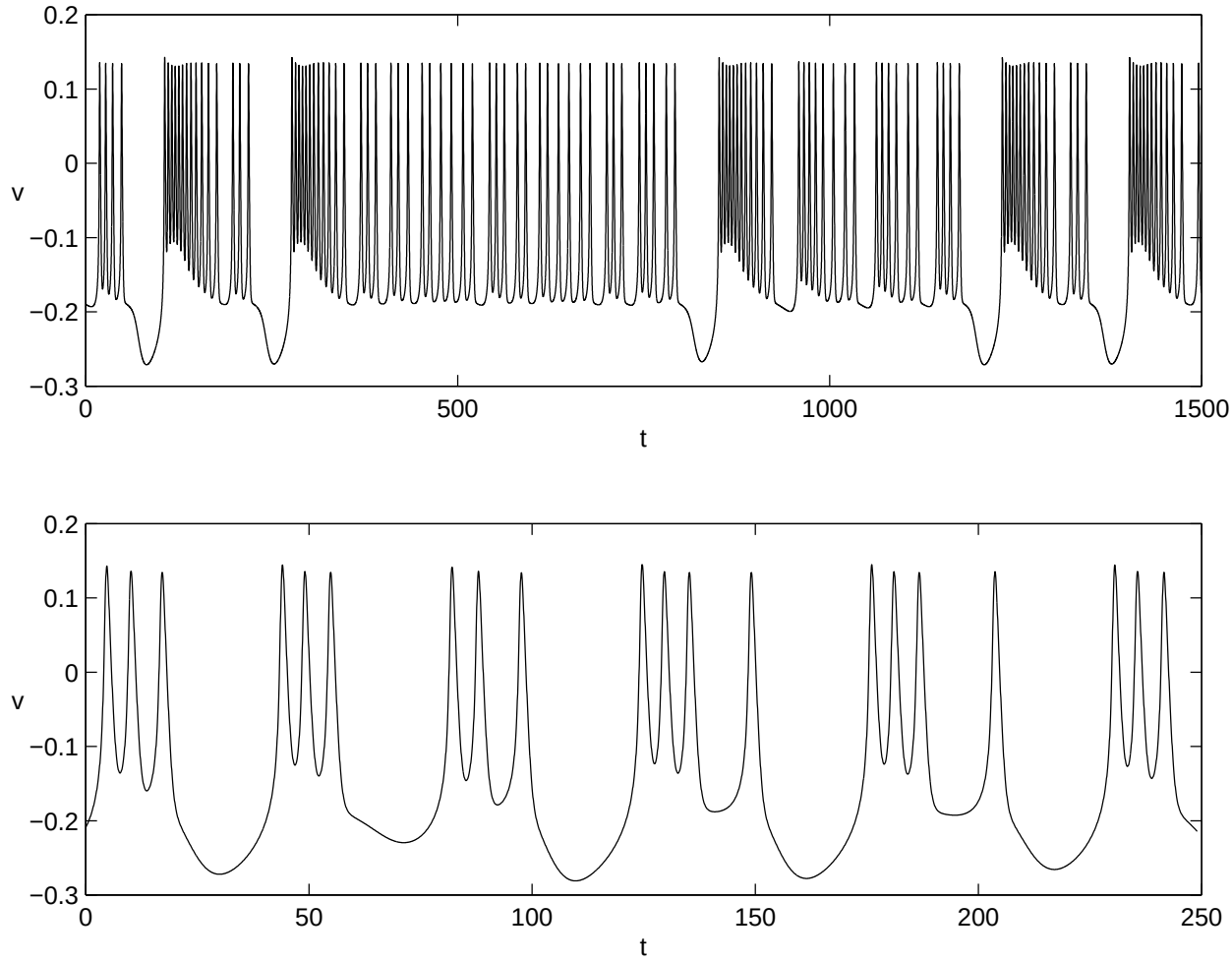

Figure 3: Chaotic dynamics from the square-wave bursting model. Note that v represents a rescaled voltage. A. (top) Chaotic solution generated by a bifurcation in λ. B. (bottom) Chaotic solution generated by a bifurcation in ϵ.

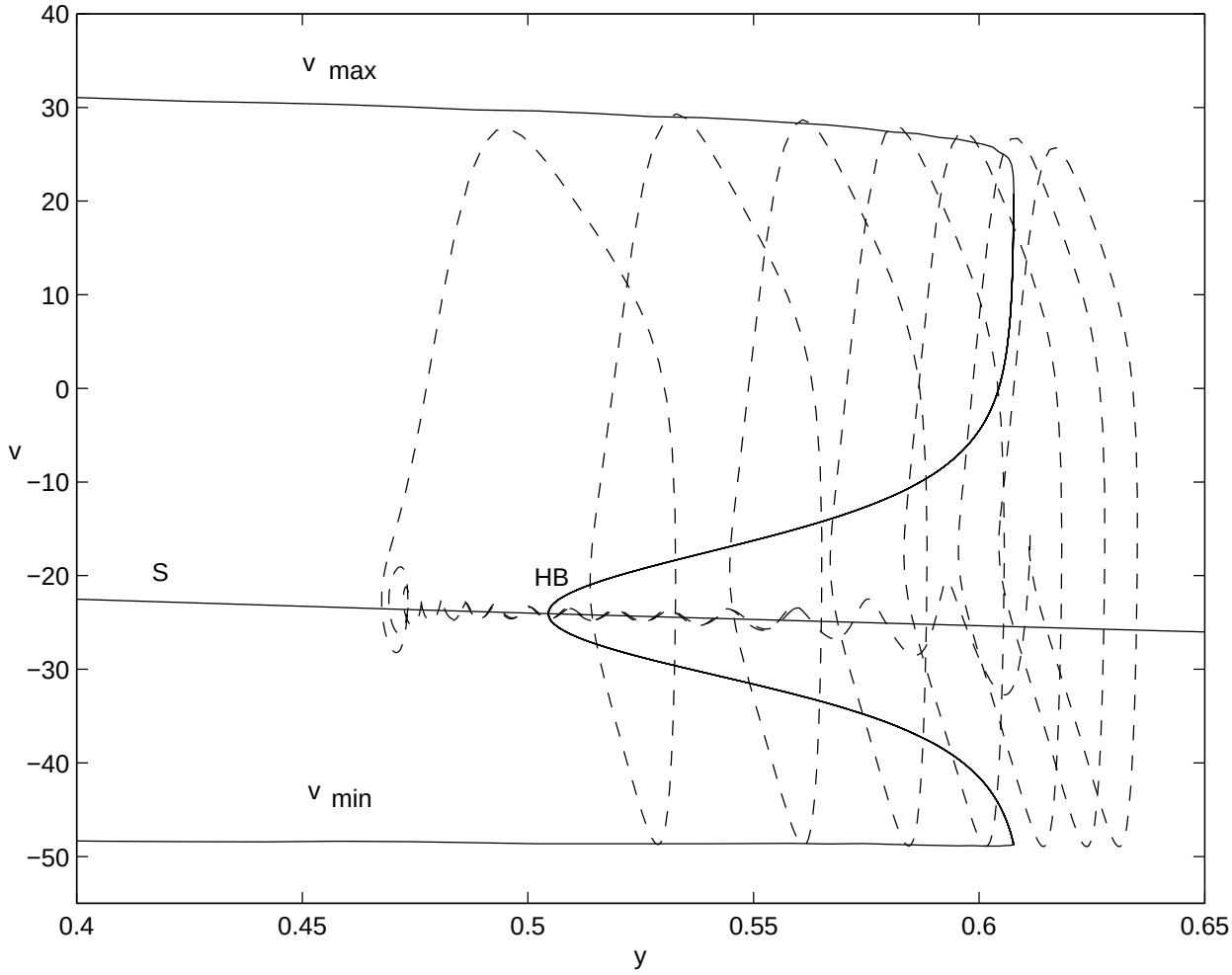

Figure 4: Bifurcation structure for elliptic bursting. The labels are as in Figure 2. The dashed trajectory is the projection of a elliptic bursting solution. This solution travels along S with y decreasing in the silent phase and then jumps up to the active phase to the left of HB.

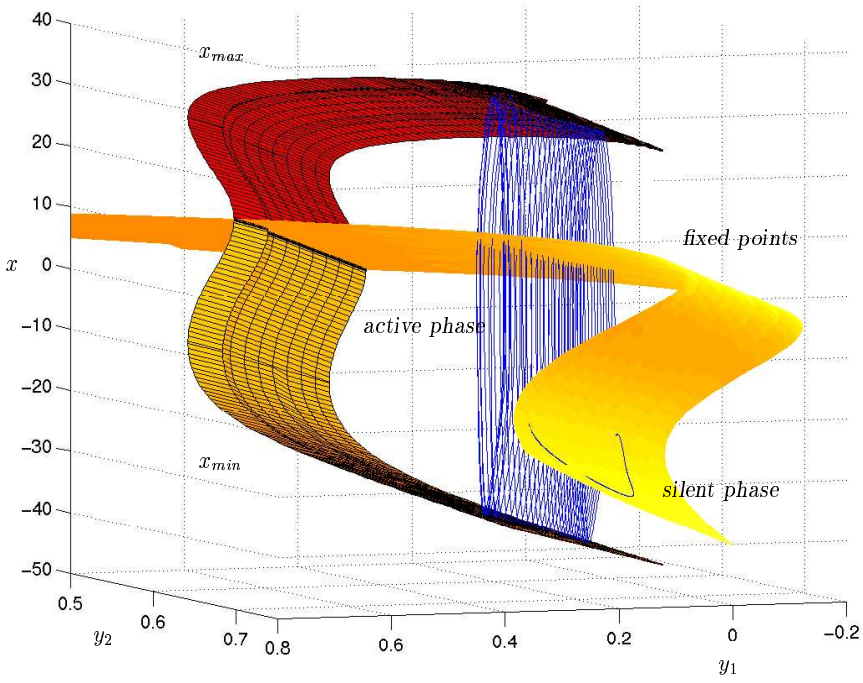

Figure 5: Bifurcation structure for parabolic bursting. Here, x denotes one component of the fast variable. The meshed surface represents the maximum and minimum x-values of periodic orbits of (FS) while the solid surface consists of fixed points of (FS). The solid trajectory is the projection of a parabolic bursting solution.

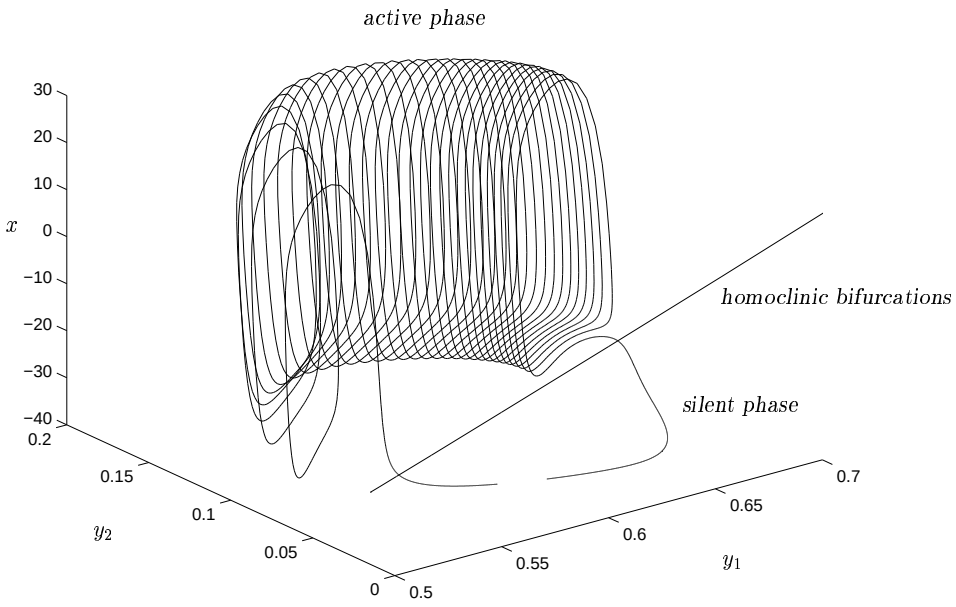

Figure 6: A projection of a parabolic bursting solution. The slow dynamics sweep the trajectory from the silent phase across the curve of homoclinic bifurcations to the active phase, where oscillations occur, and back.

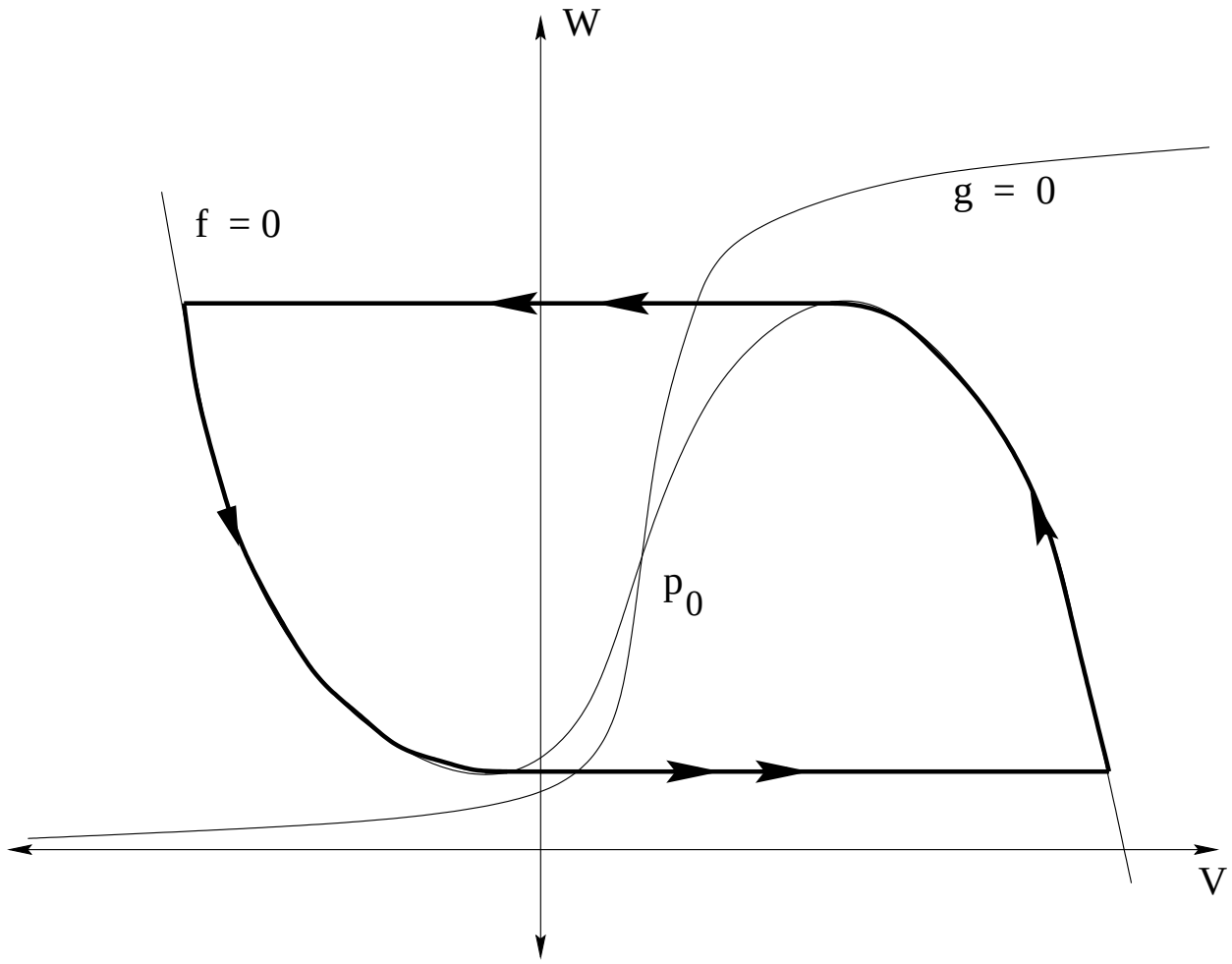

Figure 7: Nullclines and singular periodic orbit for an oscillatory relaxation oscillator.

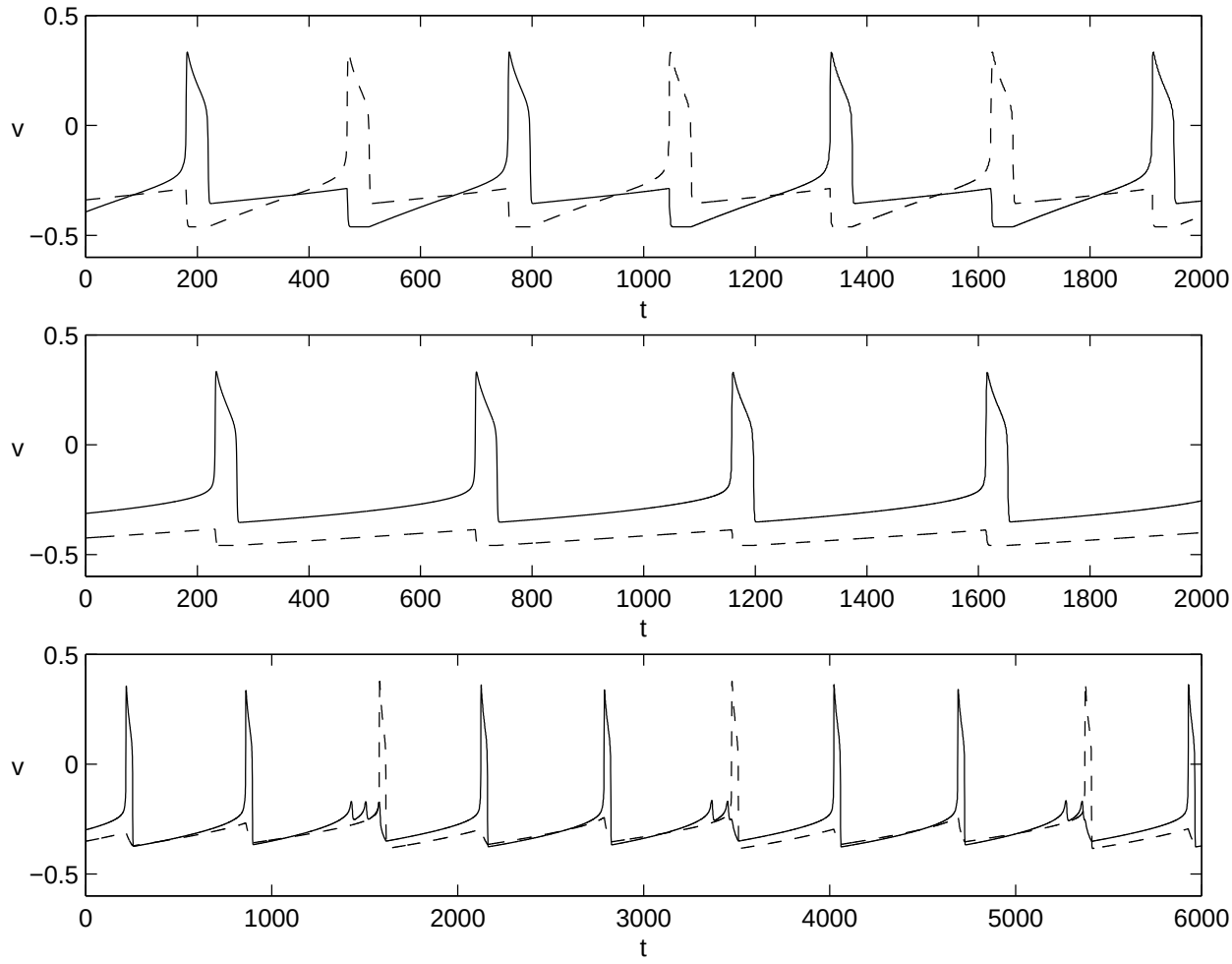

Figure 8: Nonsynchronous solutions for two mutually coupled cells [85]. Note that v represents a rescaled voltage. A. (top) Antiphase solution. B. (middle) Suppressed solution. C. (bottom) Two-to-one solution.

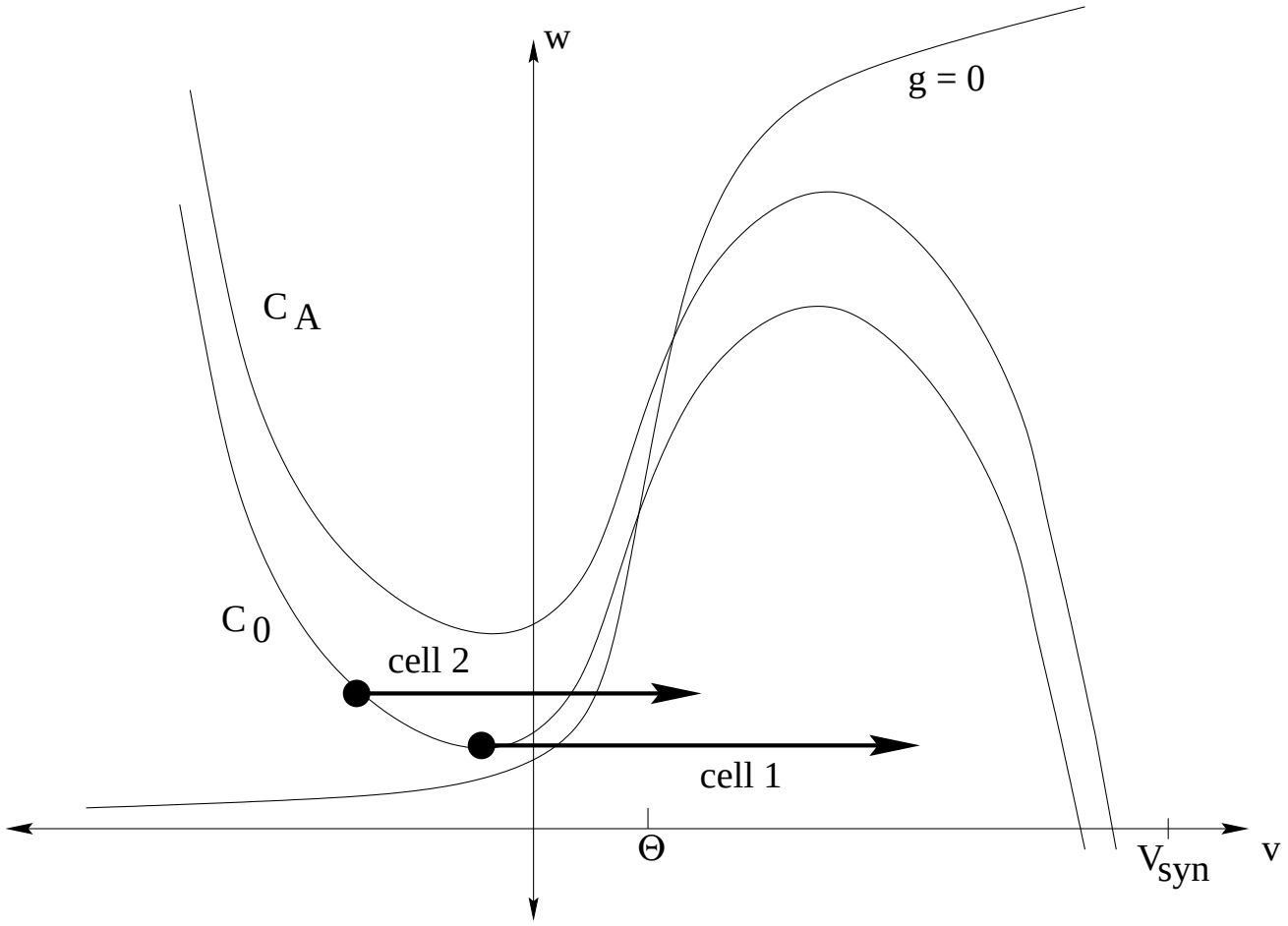

Figure 9: Nullclines for an oscillatory relaxation oscillator with (C_A) and without (C_0) excitatory coupling. Note that cell 2 responds to cell 1 through Fast Threshold Modulation.

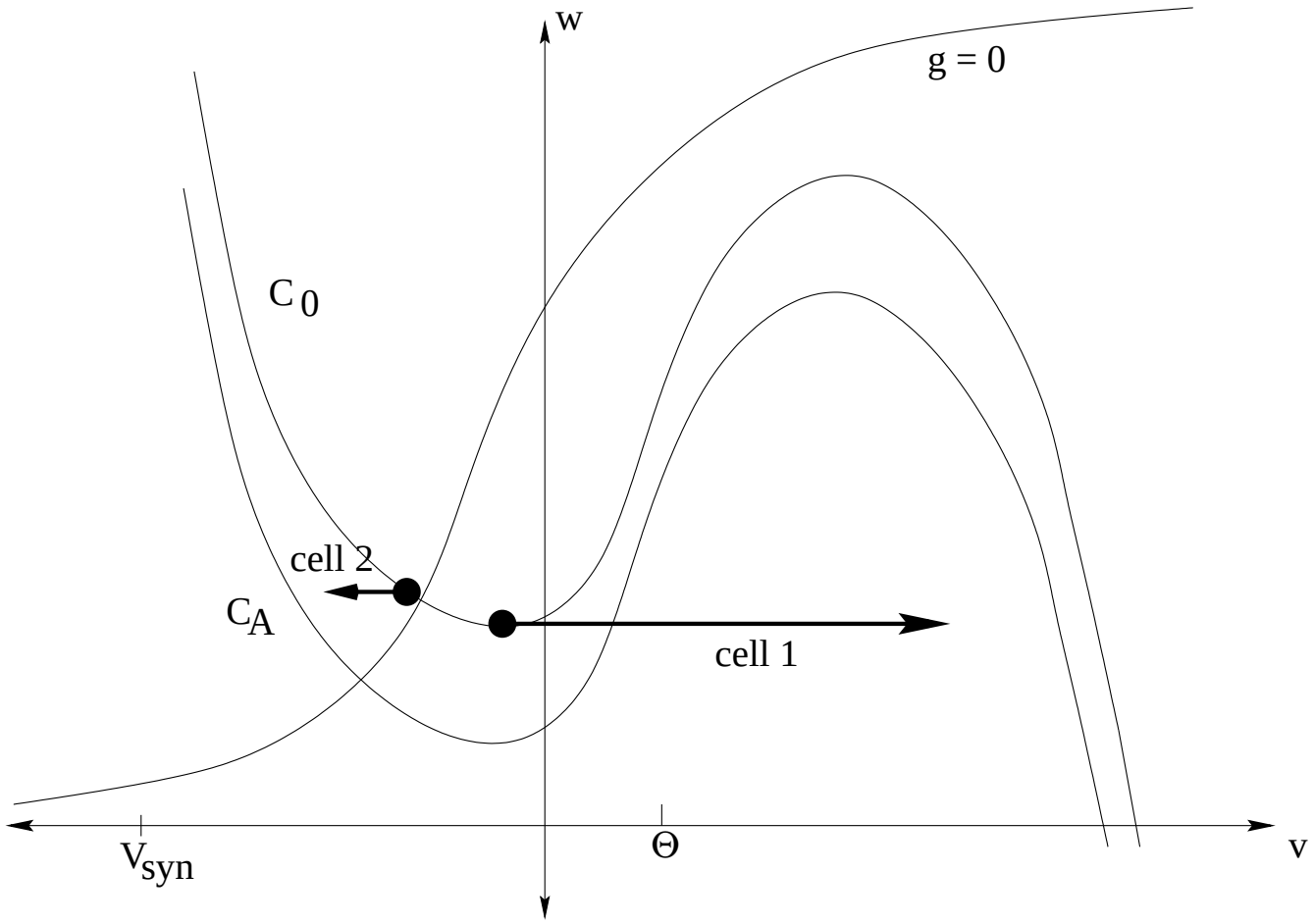

Figure 10: Instability induced by mutual inhibition. Cell 2 jumps to C_A when cell 1 fires. The excitable case is shown, while the identical mechanism leads to the instability of the synchronous state in the oscillatory case.

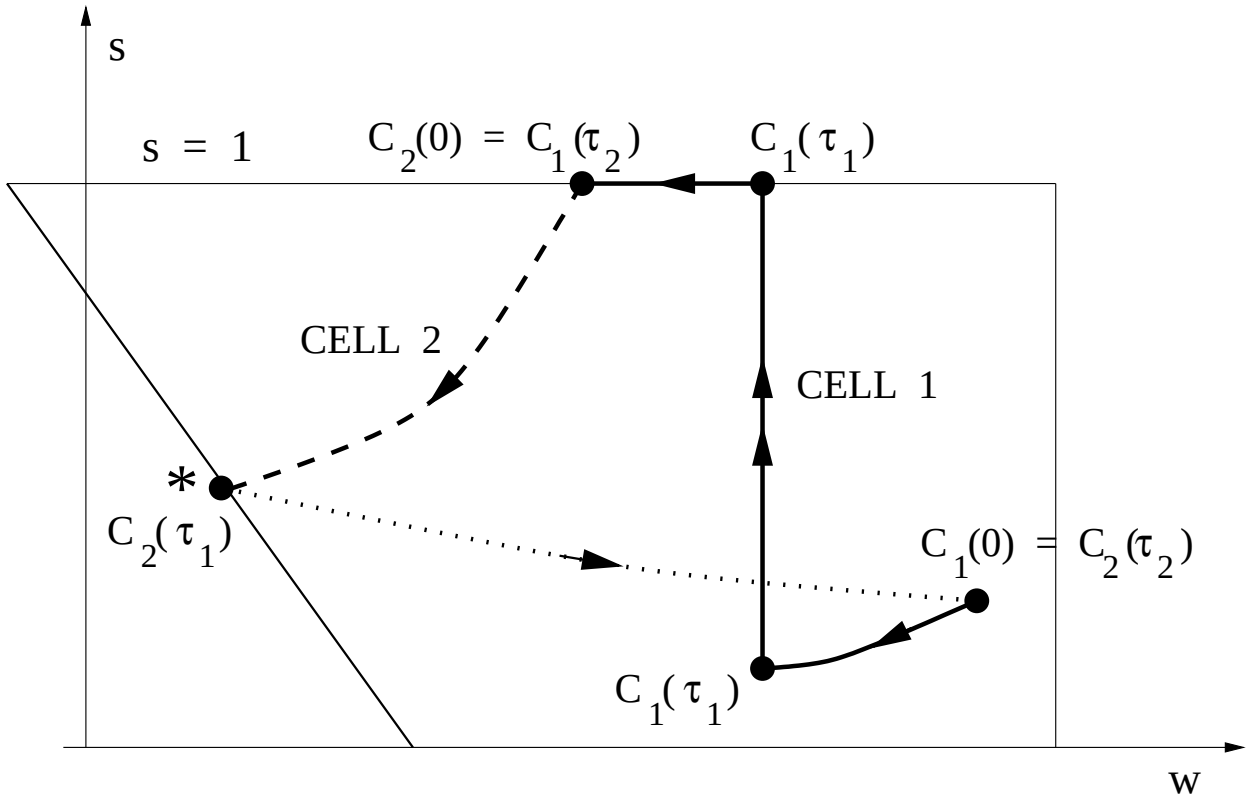

Figure 11: The projection of an antiphase solution onto (w, s) [85]. One-half of a complete cycle is shown; during this time, cell 1 remains silent (solid curve). The dashed curve shows the evolution of cell 2 in the silent phase, while the dotted curve shows its evolution in the active phase; cell 2 jumps down at time τ_2.

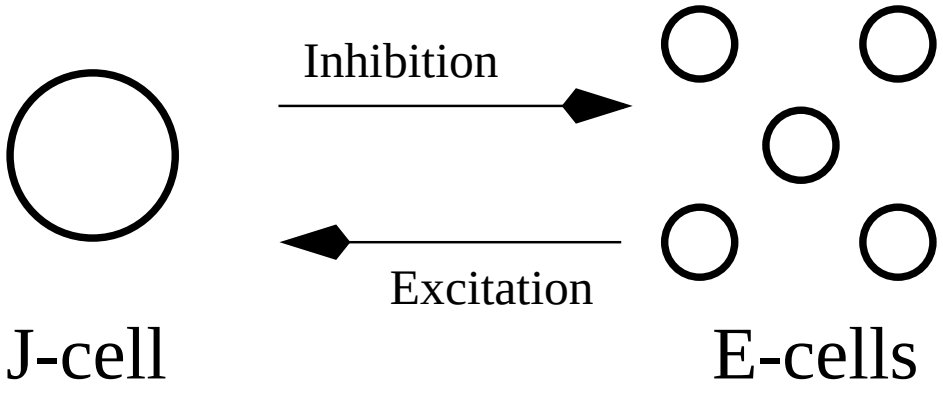

Figure 12: Globally inhibitory network. The J-cell inhibits the E-cells, which excite the J-cell.

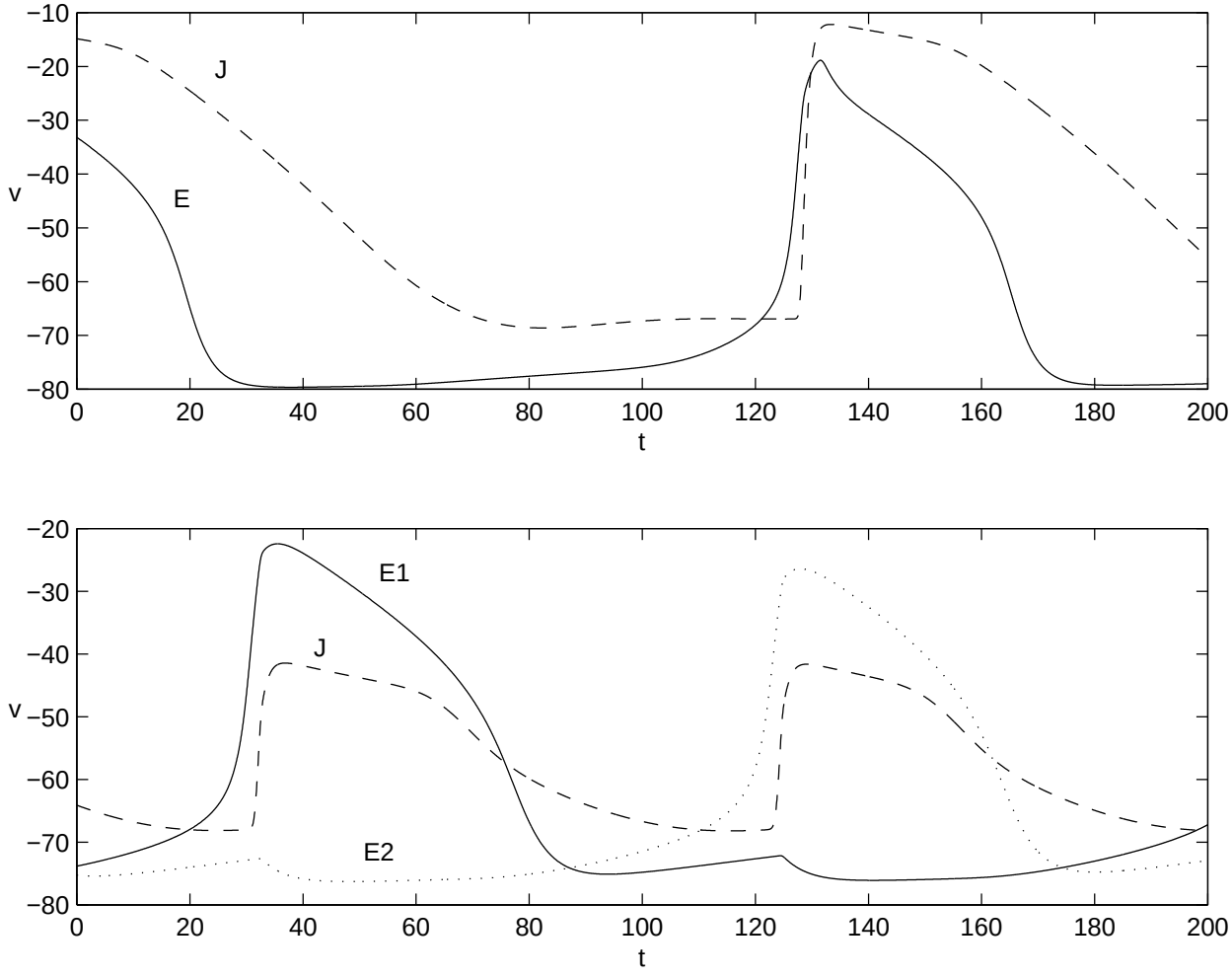

Figure 13: Solutions for a globally inhibitory network of four E-cells and one J-cell. A. (top) A synchronous solution; the solid curve is the time course of E-cell voltage and the dashed curve is the time course of J-cell voltage. B. (bottom) A 2-cluster solution; the solid and dotted curves are the voltage time courses of two different E-cell clusters of two cells each. The dashed curve is the time course of J-cell voltage. Note that the J-cell fires less powerful, shorter bursts in B than in A.

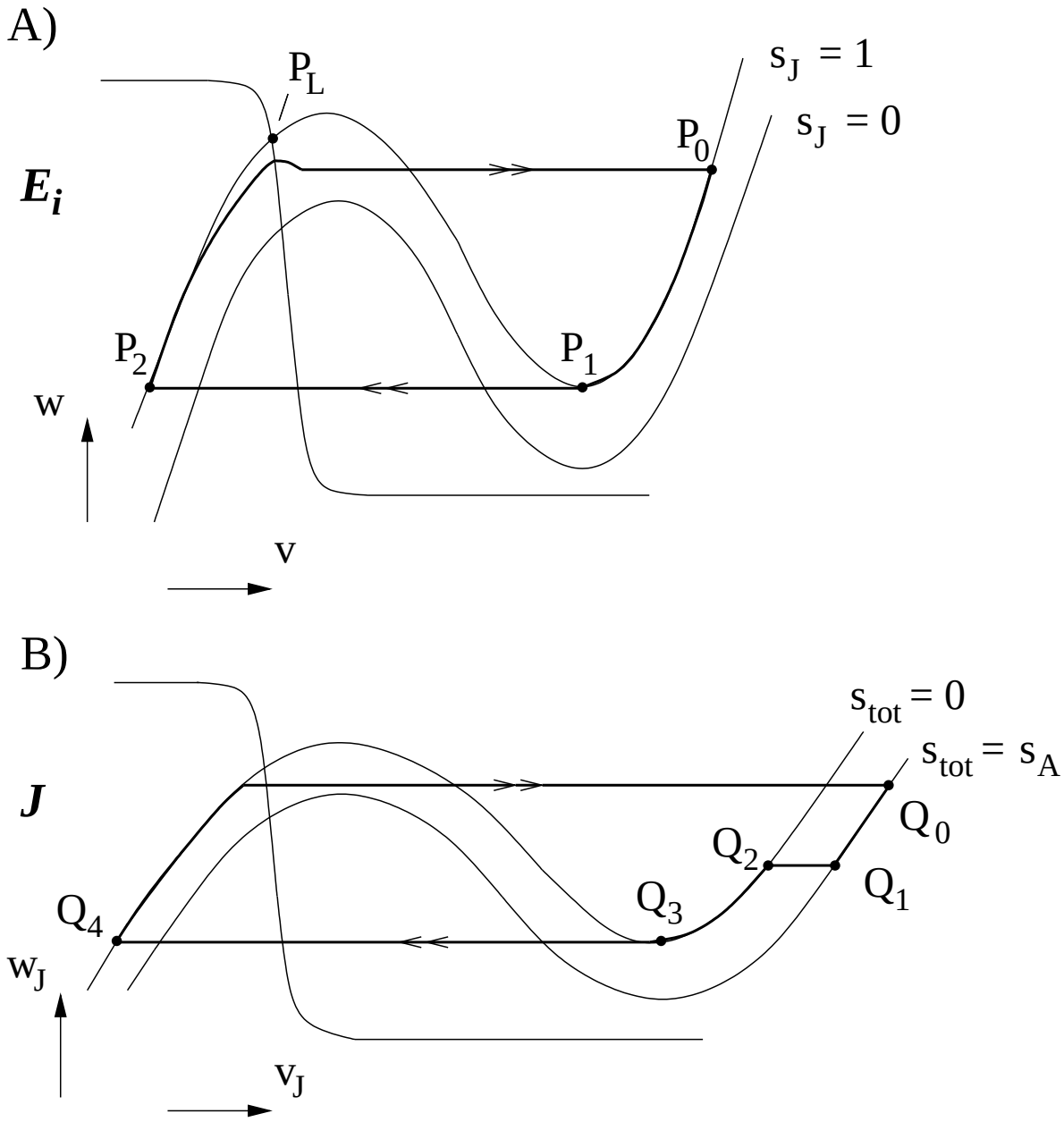

Figure 14: Nullclines for A) E-cells and B) J-cells in a globally inhibitory network [63]. The heavy lines and points P_i, Q_i correspond to the singular synchronous solution discussed in the text. Note that s_J decays on the slow time scale.

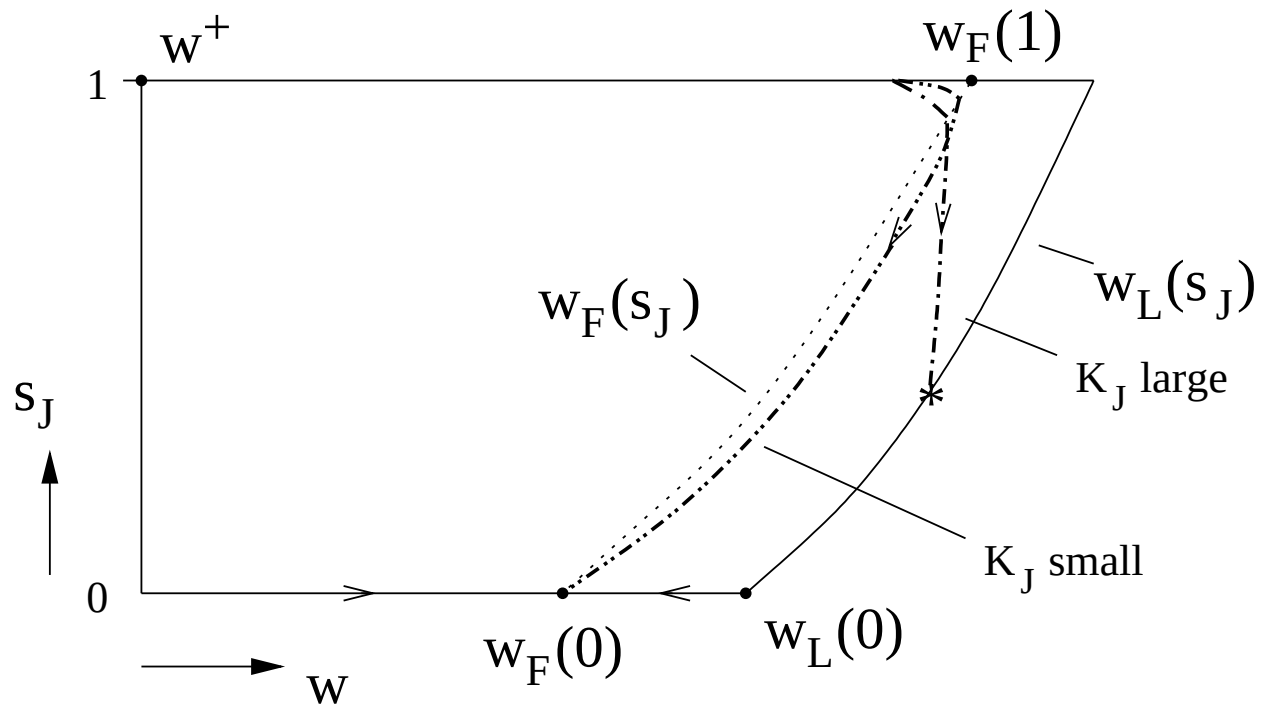

Figure 15: The slow phase plane for an E-cell [63]. The curve $w_L(s_J)$ is the jump-up curve, which trajectories reach if K_J is large enough. The dotted curve $w_F(s_J)$ consists of zeros of $G_L(w, s_J)$ in system (4.3); trajectories tend to $w_F(0)$ as $s_J \to 0$ for small K_J. Note that $w' < 0$ for $w > w_F$.